CHALMERS
UNIVERSITY OF TECHNOLOGY

Application of Suction Caissons to Submerged Floating Tunnel at Sognefjord in Norway

Caisson Design, Deflection Analysis and Physical Modelling

Master of Science Thesis in the Master's Programme Infrastructure and Environmental Engineering

YUXIANG DUAN

Department of Civil and Environmental Engineering
CHALMERS UNIVERSITY OF TECHNOLOGY
Gothenburg, Sweden 2014:104

MASTER'S THESIS 2014:104

Application of Suction Caissons to Submerged Floating Tunnel in Sognefjord in Norway

Caisson Design, Deflection Analysis and Physical Modelling

Master of Science Thesis in the Master's Programme Infrastructure and Environmental Engineering

YUXIANG DUAN

Department of Civil and Environmental Engineering
CHALMERS UNIVERSITY OF TECHNOLOGY
Gothenburg, Sweden 2014:104

Application of suction caissons to submerged floating tunnel at Sognefjord in Norway
Caisson Design, Deflection Analysis and Physical Modelling

Master of Science Thesis in the Master's Programme Infrastructure and Environmental Engineering

YUXIANG DUAN

Examensarbete / Institutionen för bygg- och miljöteknik,
Chalmers tekniska högskola 2014:104

Department of Civil and Environmental Engineering
Division of Geo Engineering
Chalmers University of Technology
SE-412 96 Göteborg
Sweden
Telephone: + 46 (0)31-772 1000

Cover:
Suction caisson applications in offshore engineering, reference to www.ngi.no/no/Innholdsbokser/Referansjeprosjekter-LISTER-/Referanser/Skirted-Caisson-Foundations-for-Offshore-Structures/

Reproservice / Department of Civil and Environmental Engineering Göteborg, Sweden

Application of suction caissons to submerged floating tunnel at Sognefjord in Norway
Caisson Design, Deflection Analysis and Physical Modelling

Master of Science Thesis in the Master's Programme Infrastructure and Environmental Engineering

YUXIANG DUAN
Department of Civil and Environmental Engineering
Division of Geo Engineering
Chalmers University of Technology

ABSTRACT

Suction caissons, which remain an innovative foundation solution in larger water depths in offshore engineering, are investigated in this thesis as foundation for a submerged floating tunnel as suggested for the Sognefjord crossing in Norway. Based on offshore engineering practice as well as site-specific conditions, laterally loaded suction caissons connected with cables are designed for various loading scenarios that combine elements such as current, cable layout, soil type, and strength profile. The design gives an overview of the caisson dimension for the submerged floating tunnel corresponding to these scenarios. Additionally, a parametric study of the static pile-soil deformation has been performed. A physical model test is designed in order to increase the understanding of the performance of these structures under dynamic lateral loading conditions. The design follows a rigorous similitude approach to arrive at an adequately scaled model test setup. Subsequently, the most important test details on the loading rig, the sample preparation and installation method are further elaborated.

Key words: Laterally loaded suction caisson, submerged floating tunnel, lateral deflection, p-y curve, laboratory modelling

Contents

Preface

I would like to dedicate my thanks to Dr. Jelke Dijkstra, for his valuable guidelines and patient supervision on my daily work on this thesis. He always delivers to me his passion on engineering, and his encouragement indeed greatly helped me dealing with problems that I am not familiar with.

Many thanks to my family for providing endless support on my study abroad, both financially and emotionally. And I do appreciate this amazing experience studying and living in Sweden, thanks to my friends, my classmates, my teachers and everybody else who shared a great time with me. Special thanks to Charles Karayan, Ti Wang, Gaby Loly, Jorge Dacosta, Larry Yang and Xun Pan for their heart-warming company.

Göteborg, June 2014

Yuxiang Duan

Notations

Roman upper case letters

A Structure projected area normal to the flow

C_d Drag coefficient

C_v Consolidation coefficient

D Pile diameter

E_{oed} One-dimensional soil stiffness

F Actual load on suction caisson

$\tilde{F}$ Dimensionless load parameter

J Dimensionless empirical constant

G Self-weight of target tunnel section

G_1 Permanent component of self-weight

G_2 Variable component of self-weight

G_s Specific solid gravity

H Horizontal component of ultimate bearing capacity under combined load; Driange path length

H_0 Initial height of slurry in tank

H_u Pure ultimate horizontal loading capacity under pure horizontal translation

K Soil permeability

L Pile length

L_0, L_1, L_2, L_3 Position parameter

N_p Loading capacity factor

$\overline{N_p}$ Average bearing capacity factor over depth

OCR Overconsolidated ratio

P Actual lateral resistance

P_u Ultimate unit lateral resistance

R_{char} Characteristic value of pile ultimate resistance

$\mathrm{R_{deep}}$ Soil resisting force on deep part

$R_d(z_p)$ Design pile resistance at padeye depth

$R_{shallow}$ Soil resisting force on shallow part

R_u Total soil resisting force

S Complete consolidation

S_u Undrained shear strength

S_{u0} Undrained shear strength of soil at surface, for NC clay

T Traffic load

T_{c-dyn} Characteristic dynamic component of horizontal cable load

T_{c-mean} Characteristic static cable pre-tension

$T_d(z_p)$ Design cable tension at padeye depth

T_{dyn} Dynamic component of horizontal cable load;

T_h Horizontal component of cable tension

T_{mean} Static cable pre-tension

T_p Rotation period of motor

T_v Dimensionless time factor

T_{v_top} Vertical component of the top cable tension

U Flow velocity

U_v Degree of consolidation

V Vertical component of ultimate bearing capacity under combined load

V_0 Initial volume of slurry in tank

V_u Pure ultimate vertical loading capacity under pure vertical translation

Z_R Depth of reduced resistance

ΔF Ultimate resisting forces on a pile segment with length ΔZ

ΔZ Length of pile segment

Roman lower case letters

a, b Coefficient coupling horizontal and vertical bearing capacity

α Cable angle to horizontal at the top end

f Current drag load

g Gravity coefficient

k Undrained shear strength gradient over depth, for NC clay

$\tilde{k}$ A parameter related to $\frac{L}{D}, J$ and $\frac{\gamma D}{S_u}$

m_v Coefficient of volume compressibility

n_H Scaling factor for height

n_L Scaling factor for length

n_γ Scaling factor for effective unit soil weight

n_{S_u}	Scaling factor for soil undrained shear strength
n_t	Scaling factor for time
n_u	Scaling factor for fluid viscosity
γ	Effective unit soil weight
γ_{dyn}	Load factor on the dynamic tension component
r_f	Effective unit weight of water
γ_m	Material partial factor
γ_{mean}	Load factor on the mean tension component
γ'	Effective unit weight of soil after sample consolidation
t	Time
μ	Viscosity of fluid
w	Angular speed
w_0	Initial water content of clay in tank
w_1	Final water content of clay in tank
w_l	Liquid limit of soil
y	Actual lateral deflection
y_c	Reference displacement
$\tilde{y}$	Dimensionless displacement parameter
ρ_f	Fluid density
ϵ_{50}	Strain which occurs at one half the maximum stress on laboratory unconsolidated undrained compression tests of undisturbed soil samples
σ_v'	Effective vertical stress
$\Delta\sigma'$	Increment of vertical load on soil specimen

1 Introduction

1.1 Background

Aiming to guaranteeing the trade and industry along the coastal region of Norway, the Norwegian Public Road Administration has launched the project "Coastal Highway Route E39", trying to build a ferry free road from Kristiansand to Trondheim (Statens Vegvesen, 2013). To achieve it, eight currently being operated ferry crossings will be replaced by fixed road infrastructure. Among the eight fjords the Sognefjord, see Figure 1, remains the most challenging site to build transportation infrastructure due to its extremely large width and depth, around 4000 m and 1300 m respectively, therefore new concepts for bridges and tunnels need to be developed. Till now, the joint forces from international teams have conducted feasibility study on mainly three concepts: a suspension bridge, a floating tunnel, and a combination structure.

The submerged floating tunnel suggested by Reinertsen Olav Olsen Group (2012) consists of two parallel submerged concrete tubes with an outer diameter of 12.6m, and each tube has one traffic lane as well as one emergency lane in the same traffic direction, see Figure 1 and Figure 2. The two tubes are connected by diagonal bracings, which enable the two tunnels as a whole to resist environmental loadings. Sixteen steel pontoons with dimension of 26 m*80 m*8 m (width*length*diameter) are distributed at the water surface, while circular shafts are set to provide connection between the pontoons and tubes.

The tubes are subjected to complex combination of loadings, i.e., gravity load, traffic load, buoyancy, wind load, tidal load, current load, wave load, snow and ice load, deformation load (temperature etc.) and ship collision loads (Reinertsen Olav Olsen Group, 2012), thus making the tubes tend to move both horizontally and vertically. From the drivability and tunnel serviceability considerations, it becomes necessary to position the tubes so that they don’t move too much in each direction. Due to deep water and complex environment that the tunnels are exposed to, offshore oil and gas industry experience can be adopted to this project in terms of stabilizing the tubes in water. One common offshore deep-water positioning strategy is to anchor floating structures to seabed through mooring cables and suction caissons (Huang, Cao, & Audibert, 2003).

Suction caissons, also called suction anchors or suction piles, are large and hollow cylinder piles, with the top closed and the bottom open-up (Andersen, o.a., 2005; Huang, Cao, & Audibert, 2003; Aubeny, Murf, & Moon, Lateral undrained resistance of suction caisson anchors, 2001), see Figure 3. Typical suction caisson has a length to diameter ratio of six or less (Andersen, o.a., 2005). A suction anchor is able to resist both vertical and lateral loadings, which are applied to the suction anchor through mooring cables that are fixed to a point on the caisson.

Figure 1 - An overview of the Sognefjord crossing on the E39 Route, extracted from Reinertsen Olav Olsen Group (2012)

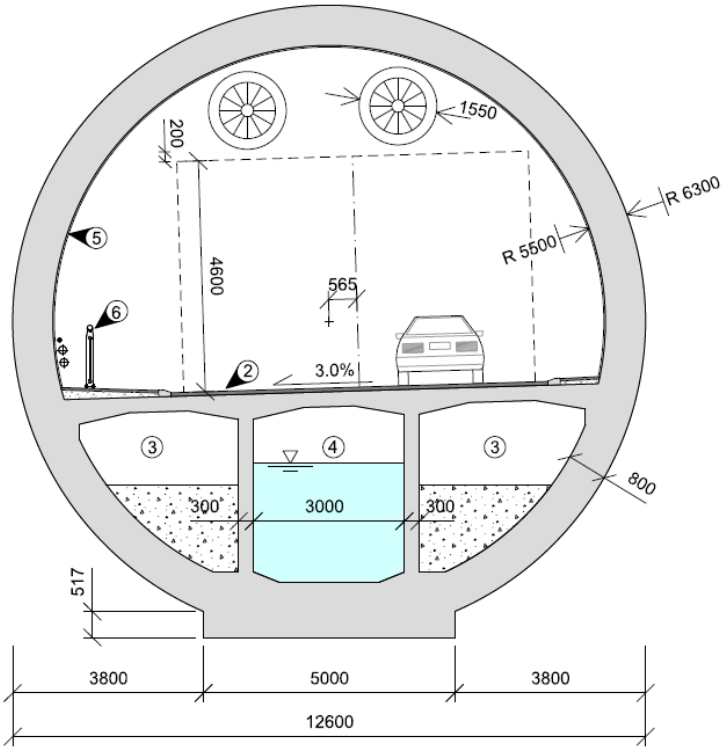

Figure 2 - Floating tunnel tube cross-section, extracted from Reinertsen Olav Olsen Group (2012)

Figure 3 - Suction caisson examples (NGI, 2014)

The name of 'suction caisson' comes from the method of installation of such caisons, which is typically driven by the pressure drawdown within the cylinder after the limited penetration due to its self-weight (Andersen, o.a., 2005; Huang, Cao, & Audibert, 2003; Aubeny, Murf, & Moon, Lateral undrained resistance of suction caisson anchors, 2001). The difference between the interior pressure and the outside water hydrostatic pressure induces a force pushing the caisson downwards besides its dead weight.

During the last decades, suction caissons have been widely used for various types of offshore facilities such as jackets and tension leg platforms, and intensive tests and practice have led to a number of experiences relating to reliable design of suction caissons (Huang, Cao, & Audibert, 2003; Aubeny & Murff, 2005). Compared with conventional driven pile foundations, suction caissons have the advantage such as relatively larger lateral loading resistance and easier and cheaper installation especially in deep water. Another advantage is that suction caissons can be precisely positioned with little uncertainty regarding anchor location and depth, if compared with other system such as drag embedment anchors. Besides, there is a trend that suction anchor is becoming larger and larger, while its application stretches into deeper and deeper water.

1.2 Objective

For the submerged floating tunnel, anchor system needs to be designed to keep the tunnel in position especially in the horizontal direction. This thesis project tries to apply offshore oil and gas experience to the design of a mooring system consisting of suction caisson foundation as well mooring cables, for the submerged floating tunnels proposed for Sognefjord crossing.

Static pile-soil deflection is also estimated empirically under possible loading conditions. In addition to static loading the floating tunnels will be subjected to cyclic loads, e.g., tidal current loads, therefore the forces acting on the suction piles are also cyclic. Another objective of this thesis project is to design a physical modelling experiment investigating the effect of cyclic loading on the long-term response of the

suction piles, i.e. the effect of cyclic loading on soil stiffness of such a foundation. Also, the experiment will verify the empirical method predicting pile deflection under static loadings.

1.3 Scope and Limitations

First of all, a simplified version of floating tunnels instead of the original one proposed by Reinertsen Olav Olsen Group (2012) is used as a basis for suction anchor design and cyclic effect analysis, see Figure 4. In this simplified structure configuration, pontoons and horizontal bracings are omitted, and the tubes, the traffic and the mooring lines as a whole is thought able to keep stabilization in the vertical direction due to the self-balance of its gravity and buoyancy. Besides, the two tubes are separated with a distance so that they have no effect on each other and can be regarded as totally independent tubes. The simplification benefits since it makes the environmental condition less complex, reducing some environmental loadings such as wind loads and wave loads to a level that they can be neglected, see Chapter 2. In summary, the structure only contains two separate tubes. In a future work, the whole tunnels should be considered as a structural system and all environmental loads should be quantitatively evaluated.

Moreover, the investigated seabed soil in this thesis is limited to marine clay as it is the most likely case, and the clay is regarded to be a deep and uniform layer containing either normally consolidated clay or uniform clay.

The design limits to focus on the pile dimension that is needed to only fulfill the requirement on lateral bearing capacity. The coupling between vertical and lateral loading capacity should be considered in a future work where both these two elements matter. The project will design different suction pile dimensions, under various conditions such as different return-period tidal current events, different cable configurations and different soil strength profile. The results will give a direct view of how current event, mooring cable and soil properties affect the designed pile dimension. Besides, the static pile-soil interaction will be estimated empirically to provide a direct view of the magnitude of deformation.

In terms of effect of cyclic loadings on pile deflection, this thesis will limit to design physical modelling experiment investigating the effect of cyclic loading on stiffness of uniform clay of suction caisson foundation, including experimental rig design, sample preparation steps, consolidation method and loading strategy. Exact loading tests will not be included in this thesis project since it takes another time period of several months.

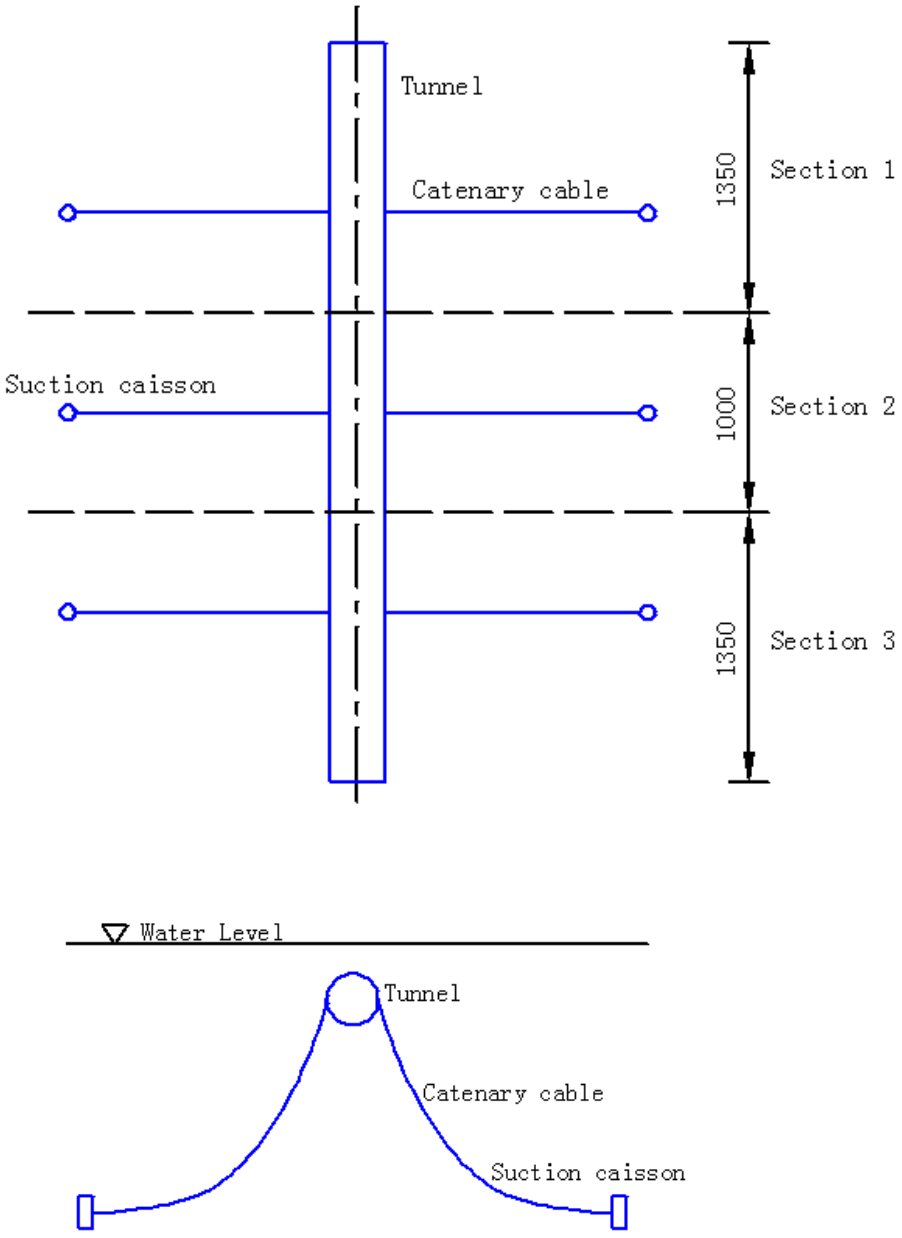

Figure 4 - Top view and side view of the anchor system configuration for one tunnel tube

1.4 Methodology

The first step is to, based on experience from offshore engineering practice, roughly design suction piles for the simplified floating tunnels. Firstly, calculate the loads on the whole structures, estimate suction pile locations and derive the lateral loads on the suction piles based on recommendation and guideline such as *Handbook of Offshore Engineering* (Chakrabarti, 2005), *Recommended Practice for Planning, Designing and Constructing Fixed Offshore Platforms—Working Stress Design, 21st edition* (API, 2005) and *Geotechnical design and installation of suction anchors in clay* (DNV, 2005).

Secondly, based on pile lateral resistance theories, apply DNV (2005) as well as API recommendation (2005) to iteratively design the proper pile dimension that is capable of withstanding environmental loading effect under different combinations of current event, mooring cable layout and soil strength. The pile dimensions required for lateral resistance are compared for these various conditions.

Thirdly, perform a pile-soil interaction analysis using the well-established p-y (unit pile lateral resistance-deflection) curve method, which is recommended by API (2005). The analysis is conducted and the results under various combinations of pile dimension, soil profile and loading conditions are compared.

At last, to evaluate the effect of cyclic lateral loading on soil stiffness, a proper laboratory experimental modelling is designed based on previous work done by Gue (1984), Santa Maria (1988) and Martin (1994). The experiment rig is thought capable of applying cyclic lateral loading to the properly scaled suction caissons in laboratory.

2 Load analysis

The submerged floating tunnel is subjected to complex environmental loadings, and this chapter will deal with the evaluation as well as calculation of the loadings on the floating tunnels.

Since the two tubes are separated and considered individually, only one tube is taken for analysis in this thesis project while the other one could be easily analyzed in the same way. For the 3700 meters long, straightforward submerged tunnel, three almost evenly distributed locations are preliminarily decided to place mooring cables anchoring to the bottom, see Figure 4 (not to scale). To simplify the analysis, environmental condition such as wind, current and wave, can be regarded as uniformly distributed along the fjord width, therefore the environmental loadings on the tubes correspondingly follows an even distribution over the tunnel, making it reasonable to assume that each set of mooring cables and suction anchors is subjected to the loadings on one specific tunnel section close to it. For instance, the mooring cables and suction piles installed in the middle of fjord is only in charge of tunnel section 2 with a length of 1000 meters, thereby the design of suction piles at this location will only depend on the loads applied on this tunnel section.

Based on the assumption above, suction piles can be designed for the three tunnel sections under the same principle, but this thesis project will only deal with the suction caissons for tunnel section 2. For the targeted tunnel section, assuming that at the longitudinal direction the loads are always balanced between traffic friction and edge-forces at the two ends of the section, the loading analysis can be simplified from 3D to 2D, meaning that the load is analysis in the vertical plane.

More precise and careful evaluation of the loadings should be achieved in a future work beyond the simplifications and assumptions made in this thesis work, to achieve more accurate design and analysis.

2.1 Self-weight

According to the data published in the Feasibility study for crossing the Sognefjord Submerged Floating Tunnel (Reinertsen Olav Olsen Group, 2012), self-weight includes two components-permanent self-weight G1 and variable self-weight G2. In this project, G_1 covers the weight of concrete tube, structural elements in tunnel, ballast, equipment and pavement, while G_2 refers to the weight of water absorbed by concrete and solid ballast as well as the weight of vegetation growth on structures. The results for all these items are summarized in Table 1, which is extracted and adjusted based on the work done by Reinertsen Olav Olsen Group (2012). The maximum self-weight is taken as the value for static analysis. Note that the water ballast in this project is primarily chosen as 100 kN/m, and it can be adjusted to control the balance in the vertical direction.

For the 1000 m target tunnel section, the gravity is

$$\boldsymbol{G} = (967 + 20 + 76 + 100 + 19 + 20 + 8 + 11 + 1) * 1000 = 1222000 \text{ kN}$$

Table 1, tunnel weight calculation

Item			Per tube (kN/m)
$\boldsymbol{G_1}$	β_1	Calculated weight of tube	967
	β_2	Calculated weight of structural elements in tunnel	20
	$\beta_{3,1}$	Weight of permanent solid ballast	76
	$\beta_{3,2}$	Weight of relocatable water ballast	100
	β_4	Weight of permanent pavement	19
	β_5	Weight of permanent equipment	20
	sum		1202
$\boldsymbol{G_2}$	β_6	Weight of marine growth	8
	β_7	Weight of water absorbed by concrete structure	11
	β_8	Weight of water absorbed by solid ballast	1
	sum		20

2.2 Traffic load

The distributed vertical loading from traffic is extracted from Feasibility study for crossing the Sognefjord Submerged Floating Tunnel (Reinertsen Olav Olsen Group, 2012) table 4-4, and the result shows it is 10 kN/m. For the 1000 meters long tube, the evenly distributed load accumulates to

$$T = 10 * 1000 = 10000 \text{ kN}$$

2.3 Buoyancy under tide

The tunnel is totally submerged in water, so the buoyancy can be determinated through Archimedes Principle, i.e.

$$Buoyancy = \rho g V \quad (1)$$

where ρ =fluid density, 1000 kg/m^3;

g =gravity coefficient, 10 N/kg;

V =volume of tube.

With an outer radius of 6.3 m, the buoyancy on the 1000 meters long tube section equals to

$$\text{Buoyancy} = \rho g V = 1240926 \text{ kN}$$

The buoyant load stays constant due to the invariable submerged volume, however the distance from the submerged tube to water surface do vary periodically as tide causes

periodic water level rising up and going down and thus leading to a fluctuating tidal current drag force, as illustrated in Chapter 2.4.

2.4 Tidal current drag force

The current considered here-tidal current, is strongly coupled with tide, which means that the horizontal movement of water (current) is closely related to the water vertical movement (Kartverket, Currents, 2014a). The current coupled with a rising tide is named 'flood' and the current occurring with a falling tide is called 'ebb'. Due to the lack of data, it is assumed that at the crossing site the current moves towards the fjord at rising tide and outwards at falling tide, just like the situation at the mouth of the Sognefjord. In other word, the current flow switches direction immediately at highest/lowest tide.

Flow velocity or current strength, often follows a distribution over water depth, with higher value near the surface and lower value at depth (Chakrabarti, 2005). The current will induce varying pressure around the concrete tube, imposing drag force on the tube in the direction of water flow. The drag force on the tunnels depends on fluid density, flow velocity and the projected area of the tube normal to the current flow:

$$f = \frac{1}{2}\rho C_d A U^2 \qquad (2)$$

where f =current drag load

ρ =fluid density, 1015 kg/m^3;

C_d =drag coefficient, here is taken as 0.75 as a conservative value according to Reinertesen Olav Olsen Group (2012).;

A =structure projected area normal to the flow, m^2;

U =flow velocity, m/s.

Since current flow switches directions regularly in the fjord, flow velocity varies periodically and thus causing the current drag force cyclic. The flow velocity depends on water depth, so the tide-induced water level variation matters in terms of determining flow velocity and drag force. Due to the lack of precise data at Sognefjord, tidal level record at Ålesund is adopted according to the recommendation from Reinertsen Olav Olsen Group (2012).The data published shows that the tide period in Ålesund is around 12 hours and 25 minutes (Kartverket, Tide table, 2014b) and that for a 100 year return period tide event, lowest, mean and highest water level reach -0.38 m, +1.2 m and +3.05 m respectively (Kartverket, Tidal Level – Ålesund, 2014c). Assume that the tunnel centre stays at 26.3 m below mean water level (+1.2 m), the possibility for the occurrence of a ship collision will be quite low. A table summarizing some important tidal levels in Ålesund is extracted from Kartverket (c) and shown in Table 2, where the lowest and highest water level observed ever since 1993 estimates a 100 year return period tide event.

Table 2 - Tidal level in Ålesund referred to lowest astronomical tide

Return period	Water level referred to lowest astronomical tide (cm)		
	high	mean	low
100 year	305	120	-38
1 year	261	120	-10

Normally the 100 year return period tide can be considered in combination with a specific return period of current event, but in this way it will introduce two time-varying parameters, i.e., flow velocity and water level. To simplify the problem, here the time-varying water level is neglected, i.e., the water level is set fixed to mean water level +1.2 m all the time, hence flow velocity distribution becomes the only considered parameter that varies with time. The concrete tube center lies 26.3 meters below the mean water surface, and the velocity at that depth can be easily obtained providing the velocity profile and can be regarded as the mean flow velocity for the whole tunnel, which is used to calculate the drag force on the tunnel as shown below.

The 50 year return period current velocity profile is extracted from table 5-1 in the document *Sognefjord Feasibility Study of Floating Bridge* (Aas-Jakobsen, Johs Holt, NGI, & Skanska, 2013) and is shown in Table 3. The velocity at depth 26.3 m is interpolated between that at depth 10 m and at depth 30 m. This document also claims that within a measurement duration of 400 days the maximum current velocities at surface and 20 meters deep are 0.77 m/s and 0.35 m/s respectively, so in this thesis project these values are taken corresponding to a one year return period current event (see Table 4), where the velocity at depth 26.3 m is extrapolated between that at depth 10 m and at depth 20 m.

The drag force on the target tunnel section has been calculated and displayed in Table 3 and Table 4.

Table 3 - 50 year return period current velocity profile

50 year return period current		
Velocity(m/s)	0-10 m	1.25
	26.30 m	0.80
	30 m	0.7
Drag force	kN/m	3.083
Total for 1000m tunnel section	kN	3083

Table 4 - 1 year return period current velocity profile

1 year return period current		
Velocity(m/s)	0-10 m	0.77
	26.30 m	0.22
	20 m	0.35
Drag force	kN/m	0.227
Total for 1000m tunnel section	kN	227

2.5 Wave loads, wind loads and others

Due to the very deep submergence of the tunnel (26.3 m below mean water level), wave and wind is unlikely to impose large load effect on the concrete tube, so these loadings are neglected in this project.

Other loads include vortex induced vibration, ice and snow loads, ship collision accident loads and deformation loads, and the analysis of these loads have been conducted by Reinertsen Olav Olsen Group (2012). However, these loads are omitted in this project due to their relatively small effect as well as complicated evaluation process. On the other hand, further analysis of the impact of these loads may be conducted to make the design and analysis of suction caisson more reliable.

3 Lateral suction pile design

The environmental loads analyzed in Chapter 2 tend to move the concrete tunnel, but with a mooring system consisting of cables and suction caissons, the tunnels are connected to fjord bottom thus avoiding large movement. This chapter will deal with the design of suction caissons for the submerged tunnels.

The design of suction anchor in this project is based on the principle proposed in *Geotechnical Design and Installation of Suction Anchors in Clay* by DNV (2005), which generally applies limit state method of design incorporating partial safety factors for cable line tension as well as soil resistance. The basic criteria a suction pile should satisfy is

$$R_d(z_p) - T_d(z_p) \geq 0 \tag{3}$$

Where $R_d(z_p)$=design pile resistance at padeye depth;

$T_d(z_p)$=design cable tension at padeye depth where cable attaches suction pile.

Theoretically both ultimate limit state ULS and accidental damage limit state ALS should be thoroughly considered in suction anchor design, where ULS aims to ensure that individual anchor has strong strength to resist extreme environmental load effect while ALS ensures that the mooring system has enough resistance under the situation of failure of one anchor for unexpected reasons. But this project will only focus on anchor pile dimension that is required to satisfy ULS.

3.1 Mooring Cable

Catenary lines are used to moor the tunnels to the fjord bottom, see Figure 4. Assume that the anchor cable at the lower end lies almost horizontally at depth below soil surface. According to Chakrabarti (2005), the catenary cables are thought to be subjected to tension only meaning that shear forces and bending moments are simply ignored. Besides, the horizontal component of cable tension T_h keeps constant along the cable line. From the perspective of static equilibrium of the catenary cable itself, the cable tension at the top end owns a vertical component T_{v_top} equalling to the self-weight of the whole cable.

Besides, taking into account the symmetric layout of cables at the two sides of tunnel and the static equilibrium of the concrete tube, vertical component of the top cable tension T_{v_top} at the top end of mooring cable can be easily obtained as

$$T_{v\_top} = \frac{1}{2} * (\text{buoyancy} - \text{gravity} - \text{traffic load}) \tag{4}$$

From the data from Chapter 2, we obtain

$$T_{v\_top} = 4463 \text{ kN}$$

If considering no current effect, the cable will still be in tension status and this cable load is called static pre-tension T_{mean} (strictly speaking, it should be cable pre-tension plus mean current load effect, but since mean current load is 0 it is omitted). The horizontal component of T_{mean} is the mean value of horizontal cable tension. Now considering current effect, dynamic horizontal force on the tunnel section will be balanced by the two cable strands beside the tunnel. From the symmetry point of view, this current load will increase tension in one cable and decrease the same amount of tension in another cable, i.e.,

$$T_{dyn} = \pm\frac{1}{2} * Current\ Drag\ Force \quad (5)$$

To guarantee that the cable is always in tension status which is beneficial from the perspective of constraining deformation (Andersen, Bearing capacity under cyclic loading-offshore, along the coast, and on land. The 21st Bjerrum Lecture presented in Oslo, 23 November 2007, 2009), the cable needs to have a mean tension T_{mean}no less than T_{dyn}, i.e.,

$$T_{mean} \geq T_{dyn} \quad (6)$$

Horizontal component of cable tension T_h consists of a mean value T_{mean} and a dynamic value T_{dyn}, which perceptively comes from static cable pre-tension as well as dynamic current loading effect, i.e.,

$$T_h = T_{mean} + T_{dyn} \quad (7)$$

Three conditions are known or simplified:

1. The water depth is 1250 meter.
2. The cable lies horizontally at the lower end.
3. The vertical tension component at the top end is 4463 kN.

With these conditions, assume an angle to horizontal α (Figure 5) at the cable top end when no current effect is involved, and calculate the horizontal component of pre-tension via known T_{v_top} and α, *i.e.*,

$$T_{mean} = T_{v\_top}/\tan(\alpha)$$

Furthermore, providing the general equation of catenary line (Math24.Net, 2014), calculate the line length and choose proper cable properties. The results obtained from different angles α are summarized in Table 5 while the calculation process is attached in Appendix A.

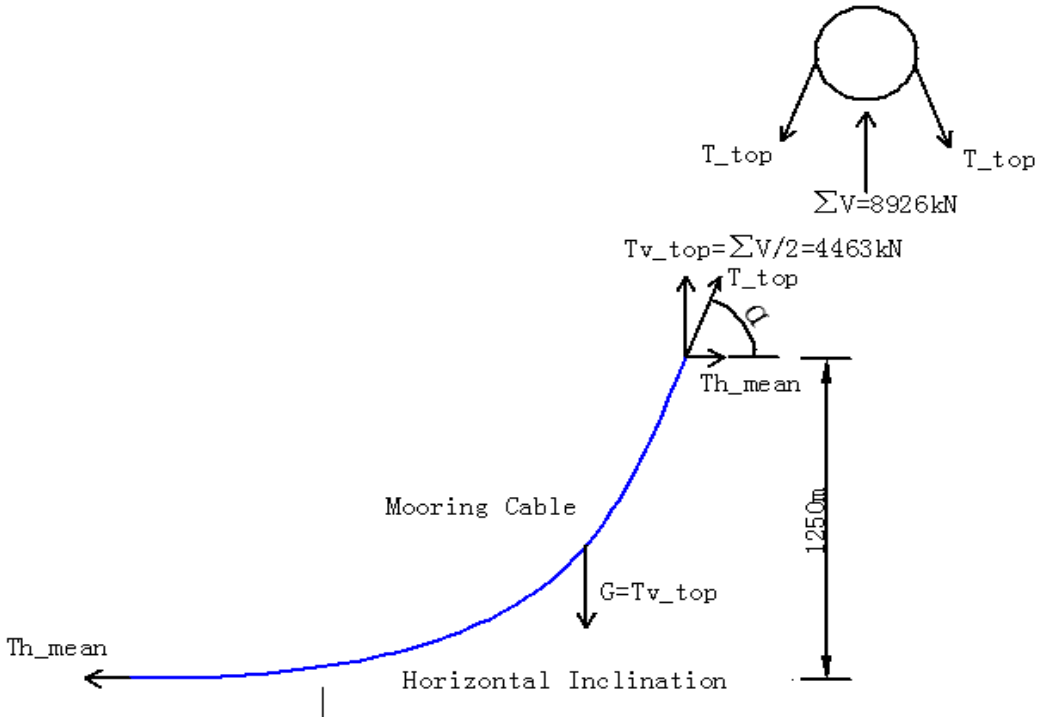

Figure 5 – Mooring cable layout

Table 5 - Mooring cable properties for different top end angles

α	T_{v_top}, kN	T_{mean}, kN	T_{dyn} by 50 year current, kN	T_{dyn}/T_{mean}	Cable dimension	Strength utilization	Cable length, m
71^0	4463	1541	1541	100%	3* D153mm	8%	1752
45^0	4463	4463	1541	30%	2* D137.5mm	20%	3020
37^0	4463	6000	1541	26%	2* D121.5mm	31%	3793

α	T_{v_top}, kN	T_{mean}, kN	T_{dyn} by 1 year current, kN	T_{dyn}/T_{mean}	Cable dimension	Cable length,m
71^0	4463	1541	114	7%	3* D153mm	1752
45^0	4463	4463	114	3%	2* D137.5mm	3020
37^0	4463	6000	114	2%	2* D121.5mm	3793

Case	Diameter, mm	Minimum Breaking Load, kN	Submerged weight,kg/m	Axial stiffness, MN
1	153	22070	95.5	2110
2	137.5	18272	77.2	1704
3	121.5	14362	59.7	1353

3.2 Design value of line tension at padeye

The design cable tension at padeye depth $T_d(z_p)$ in this project is taken as horizontal and equalling to the design value of cable tension at dip-down point $T_d(z_D)$where cable enters soil, i.e., neglecting soil resistance between the embedded cable and its surrounding soil, see Figure 6. Also, considering the dynamic characteristics of current load which changes velocity and direction periodically, design line tension at dip-down point is calculated according to DNV-RP-E303 (DNV, 2005):

$$T_d(z_D) = T_{c-mean} * \gamma_{mean} + T_{c-dyn} * \gamma_{dyn} \quad (5)$$

Where T_{c-mean} = the characteristic mean line tension;

T_{c-dyn} = the characteristic dynamic line tension;

γ_{mean} = the load factor on the mean tension component;

γ_{dyn} = the load factor on the dynamic tension component.

The horizontal dynamic line tension equals to half the dynamic current load, which has been calculated in Chapter 2.4, i.e.,

$T_{c-dyn} = \frac{1}{2} \times 3082 = 1541$ kN for 50 year return period current

$T_{c-dyn} = \frac{1}{2} \times 227 = 114$ kN for 1 year return period current

Pre-tension in the cable line depends on the cable angle α at the top end, and the horizontal component of the pre-tension at padeye has been calculated as a function of α. The pre-tension calculation is illustrated within Excel sheets in Appendix A, resulting pre-tension $T_{c-mean} = 1541$ kN, 4462 kN and 6000 kN respectively for top cable angle of 71°, 45° and 37°.

Consequence class is set as Class 1 in this project and the characteristic mean tension overweighs 2/3 of the characteristic value of dynamic tension, therefore partial factor

γ_{mean} and γ_{dyn} is chosen as 1.3 to apply to T_{c-mean} and T_{c-dyn} respectively according to DNV (2005). The design values of line tension at padeye are summarized in Table 6.

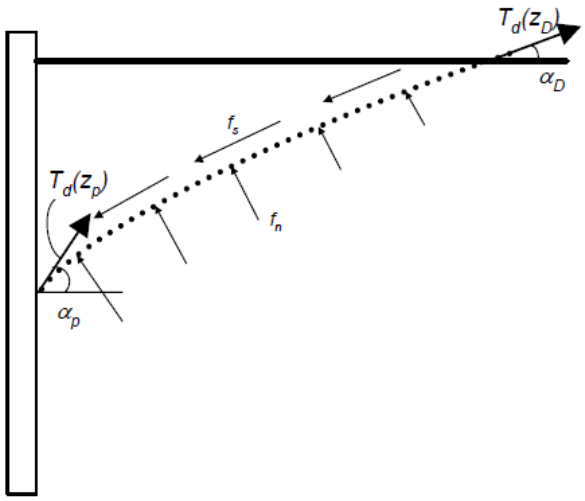

Figure 6 - Change of cable tension between dip-down point (Z_D) and padeye point (Z_p)

Table 6 Design cable load on suction caisson

Cable inclination to horizontal at top end α	Design ultimate load for suction anchors (kN)	
	50 year return period current	1 year return period current
71^0	4008	2152
45^0	7806	5949
37^0	9804	7948

3.3 Ultimate Lateral Resistance

Generally design value of ultimate resistance of a suction anchor can be calculated according to DNV-RP-E303 (DNV, 2005):

$$R_{d(Z_p)} = R_{char}/\gamma_m \quad (6)$$

Where R_{char} = the characteristic value of pile ultimate resistance;

γ_m = material partial factor and in this project is chosen as 1.2 according to table 2-1 in DNV (2005).

The critical step remains to calculate the characteristic value of ultimate lateral resistance or lateral capacity of suction caisson R_{char}.

3.3.1 General Analysis Methodology

Generally three kinds of methods are widely applied to analyse suction anchor resistance: finite element method (FEM), limit equilibrium and plastic limit analysis, and semi-empirical method (Andersen, o.a., 2005).

3.3.1.1 Semi-Empirical Method

Semi-empirical method depends on empirical rules to calculate lateral collapse load, and it tries to provide general solution for most cases, without explicitly considering any specific failure mechanisms (Andersen, o.a., 2005). One of the earliest works regarding lateral pile loading capacity is done by Broms (1964) who started with treating collapse load as ultimate unit lateral resistance distribution along the pile-soil interface and correlating the ultimate unit lateral resistance P_u to undrained shear strength S_u at that depth through a dimensionless factor N_p:

$$P_u = N_p S_u D \tag{7}$$

Where S_u = undrained shear strength;

D = pile diameter;

N_p = loading capacity factor.

Matlock (1970) and Reese et al., (1975) followed Broms's approach represented by Equation 10 and empirically proposed varying values of N_p as a function of depth. API (2005) suggested lateral loading capacity factor N_p for laterally loaded suction piles based on the work by Matlock, which remains 9 at depth and smaller close to surface The decrease of soil resistance at the soil surface is largely due to that, as pointed out by Matlock (1970), when pile is subjected to lateral load at the pile head, the soils at lower depth can perfectly confine the pile and allow a plastic soil flow in the horizontal plane but the upper soil cannot confine the pile well and the pile will then fail by shearing upwards and forwards.

Equation 10 is also adopted in plastic limit analysis to calculate lateral loading capacity of suction anchors, but with the value of N_p being obtained from analytical or numerical studies (Aubeny & Murff, 2005).

3.3.1.2 Limit Equilibrium Method and Plastic Limit Analysis

These methods both assume failure mechanisms which incorporate experimental results, analytical works, numerical studies and engineering judgement, and then approximate ultimate resistance based on plasticity theory (Andersen, o.a., 2005). But on the other hand they still gave case-specific solutions and there exists difficulty generalizing the results. Limit equilibrium method is normally used to calculate suction anchor resistance, and a reliable limit equilibrium model should properly

considers a number of factors such as actual soil strength profile, load point and load angle, set-up effect at the outer anchor wall, coupling between vertical and horizontal capacity (DNV, 2005).

Plastic limit analysis often assumes a 3D failure mechanism with some defined three-dimensional geometry at failure, and achieves the analysis based on the principle that the external work done by all the boundary and body forces equals to the internal energy dissipation during the deforming process (Murff & Hamilton, 1993; Andersen, o.a., 2005; Aubeny & Murff, 2005).

Based on empirical work from Broms (1964), Matlock (1970) and Reese et. al. (1975), Murff and Hamilton (1993) developed a more accurate model with the upper bound method of plasticity to find the lateral capacity. They assume a 3D failure mechanism in Figure 7: the pile pushes up a soil wedge in the front and creates a gap at the back side of it, with the soil below the wedge flowing in the horizontal plane around the pile. Though with the upper bound plastic method, one can directly compute the loading capacity based on energy dissipation point of view, Murff and Hamilton (1994) still applied the theory into unit soil resistance method and derived the factor $N_p = 9$ at depth which is consistent with the solution from Matlock (1970) as well as Randolph and Houlsby (1984). They also concluded that the ultimate lateral resistance has no direct correlation with whether the pile rotates or not. Later Aubeny et al. (2001) and Aubeny & Murff (2005) simplified the failure mode as shown in Figure 7, making the failure mechanism simply depending on one single variable L_0- the depth of the center of rotation.

In summary, both limit equilibrium method and plastic limit analysis estimate the upper bound failure load which gives the minimum collapse load for a specific geometry (Andersen, o.a., 2005).

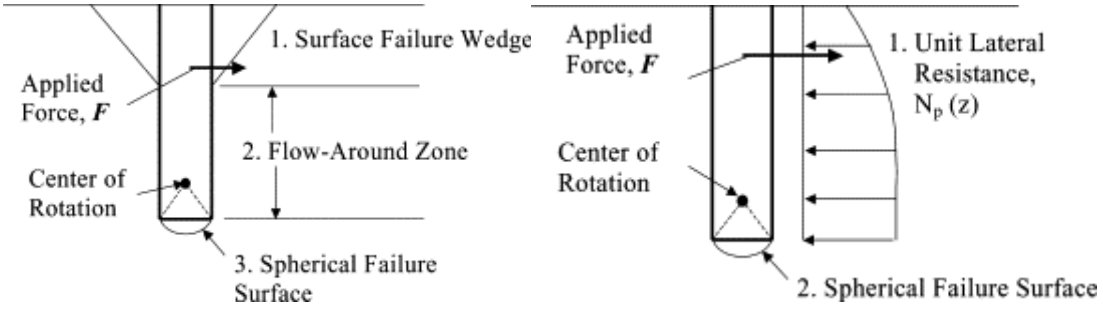

Figure 7 - Soil collapse mechanism suggested by a) Murff and Hamilton (1993), b) Aubeny et al. (2001). From Aubeny & Murff (2005)

3.3.1.3 FEM

Finite element method sets no prior assumption of failure mechanism, but automatically finds out the critical failure mode for a specific case giving all detailed information about loading and soil characteristics. It owns the advantage of modelling complex conditions like layered soils, irregular geometry, non-optimal load point, and user defined random load angle for example, but at the same time it displays disadvantages such as requiring special knowledge about numerical modelling, time consuming to build a complete model, being unable to reach general solution directly

from collapse load to pile-soil interface resistance. Apart from those above, the FEM has also been widely used to calibrate or verify other models derived from limit equilibrium method, plastic limit analysis and even semi-empirical method.

3.3.2 General Failure Mechanism and Loading Capacity

A number of failure mechanisms of suction anchors have been proposed and simplified, and experience indicates that the failure mechanism strongly depends on various factors such as location of load attachment point, loading angle, soil strength profile, ratio between pile embedment depth and diameter, the sealing condition of the anchor top cover, to name a few (DNV, 2005). Here the most important factors, load attachment position and load inclination, are fully discussed.

3.3.2.1 Load point

Load attachment point remains one important factor since it decides if the suction anchor fails by rotating, translating or both and thus influencing the loading capacity. It has been widely recognized that suction piles have the maximum loading capacity when pure translation of piles occur, without rotation involved in (DNV, 2005; Randolph & House, Analysis of suction caisson capacity in clay, 2002). This status corresponds to a special location of load attachment point- optimal load point, which is found to be around 70 percent of the caisson embedment depth (Aubeny, Murf, & Moon, Lateral undrained resistance of suction caisson anchors, 2001), see Figure 8. Compared with loading at anchor top, loading at optimal position can even result in a twice higher loading capacity according to theoretical analysis from Andersen & Jostad (1999), see Figure 8.

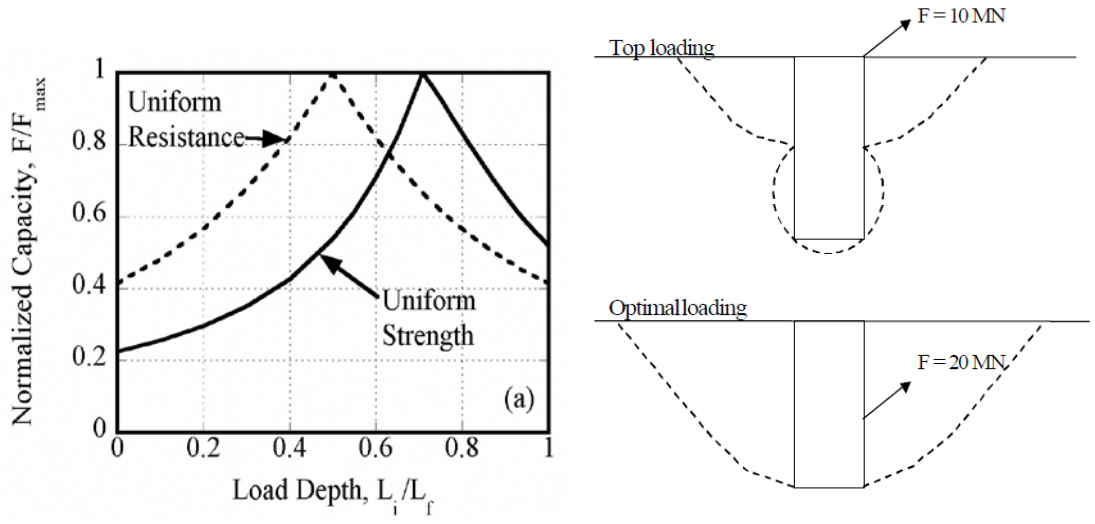

a b

Figure 8 - Effect of load position on a) capacity of uniform strength clay under apsect ratioL/D=4 (Aubeny et al., 2001) b) failure mechanism (Andersen & Jostad, 1999)

A non-optimal load point will lead to rotation of the suction anchor as well as a bit different failure mechanism with that induced at optimal load attachment point, as can be seen in Figure 8 from Andersen & Jostad (1999) and Figure 9 from Randolph & Gourvenec (2011) (for horizontally loaded suction anchors only). For an optimal load point case, the failure geometry includes a conical soil wedge and a soil flow in horizontal planes underneath the wedge, while for a non-optimal load point case the failure mode consists of a conical wedge in the surface as well as a soil zone rotating around the centre of rotation located at the lower part of suction anchor (Randolph & Gourvenec, 2011).

Besides, non-optimal position of load attachment point will decrease the loading capacity, and further the capacity can even drop dramatically providing a tension crack is formed at the active side. Though the formation of crack behind suction anchor remains difficult to be predicted, it is still recommended to consider lowering the load point beneath the optimal location (DNV, 2005).

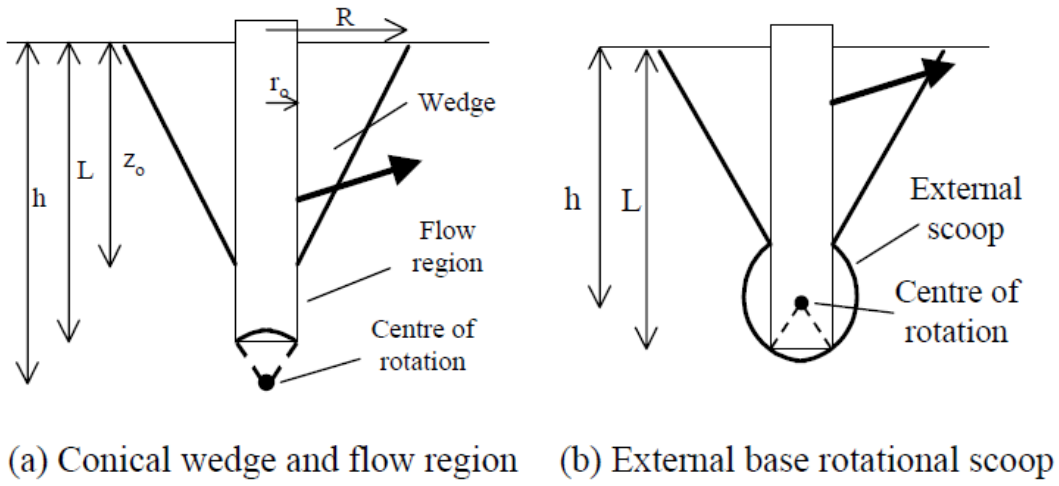

Figure 9 - Failure mechanism for laterally loaded suction anchor (a) translation mode (b) rotation mode (Randolph & Gourvenec, 2011)

3.3.2.2 Load angle

3.3.2.2.1 Vertical load

Generally when the load is almost vertical (mostly on anchor top), suction anchor will tend to be pulled out of the soil, mobilizing the soil shear strength along the outer skirt wall (DNV, 2005). Depending on anchor top sealing condition and drainage condition, soil shear strength along anchor internal wall and bottom tip resistance may be mobilized and thus causing various failure mechanisms (Deng, Carter, & Taiebat, 2001), see Figure 10. Figure 10-a corresponds to the case of anchor being loosely sealed or left open on the top; Figure 10-b is suitable for the situation when the anchor top stays at perfect sealing condition and at the same time the soil is subjected to partly drained condition so that the suction effect cannot hold more soil except for the soil plug inside the anchor; Figure 10-c refers to the mode with strict sealing top cover and limited drainage condition allowing a fully developed reverse end bearing.

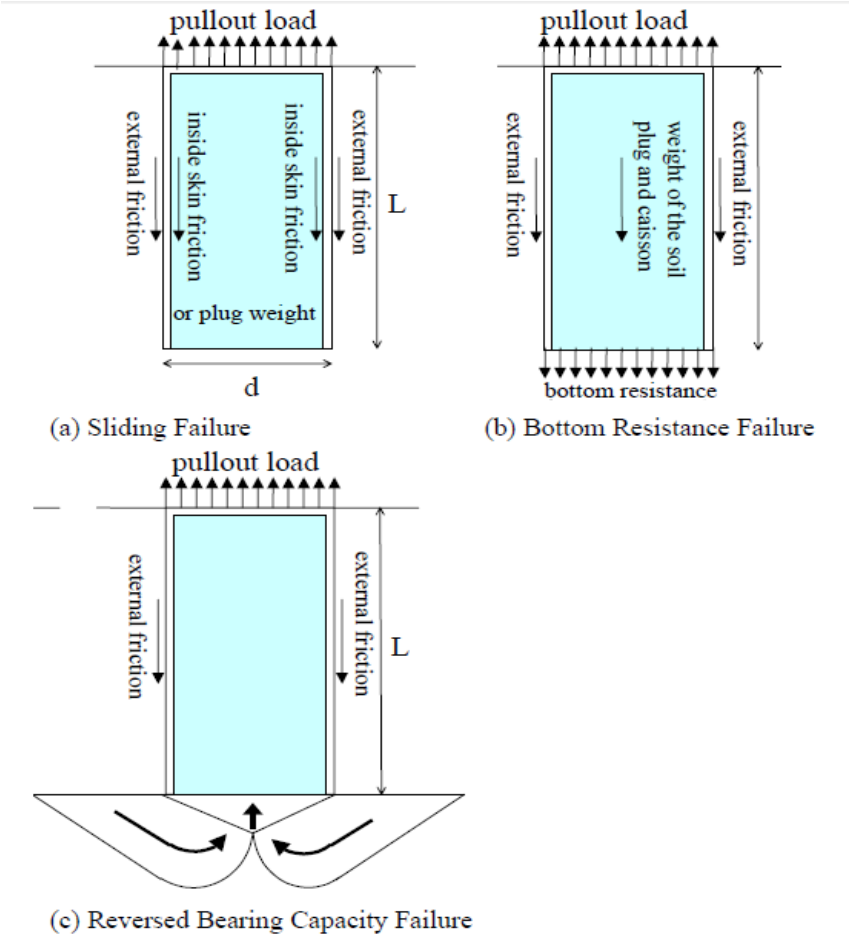

Figure 10 - Failure modes for vertically loaded suction anchors (Deng et al., 2001)

3.3.2.2.2 Lateral load

If a suction anchor is subjected to almost horizontal loads, the resistance comes from the active and passive earth pressure along the back and front sides of the pile (DNV, 2005). The failure mechanism includes a conical wedge around the anchor and perhaps horizontal soil round-flow around or below the anchor (DNV, 2005), see Figure 11-1a. Sometimes crack may be formed at the back of suction anchor but it is hard to predict, see Figure 11-1b.

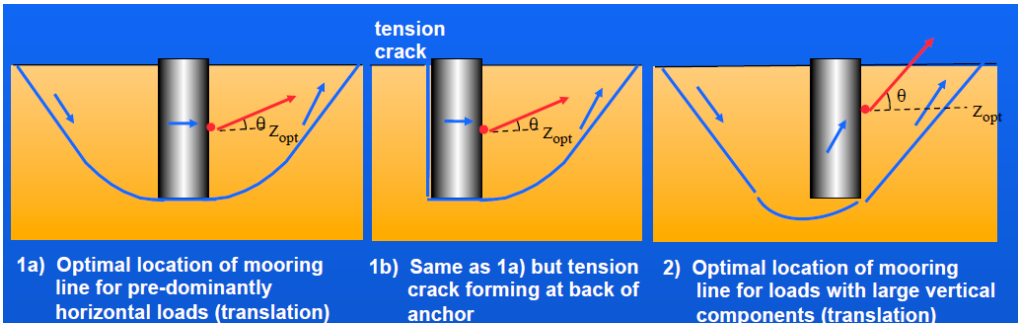

Figure 11 - Failure modes under lateral load and inclined load (TUDelft, 2014)

3.3.2.2.3 Inclined load

For inclined loading, the suction anchor may fail in a way as shown in Figure 11-2. A common recognition has been reached that there is a coupling between vertical and horizontal capacity, and the horizontal and vertical load components at failure may not reach the ultimate values which are derived at purely horizontal or vertical loads, see Figure 12-a.

Experimental and analytical studies on the interaction have been conducted by several authors. El-Sherbiny et al. (2005) made a scaled physical experiment on normally consolidated clay and graphed the interaction between horizontal capacity and vertical capacity under different loading angles, see Figure 12-b. In this figure, when the loading inclination to horizontal increases from 0 to 90 degree, the horizontal component of the collapse load will decrease from the lateral loading capacity to 0, and the vertical component will increase from a small value to the vertical loading capacity. Aubeny et al. (2003) conducted an analytical study based on plasticity theory and derived the expression of horizontal and vertical components of failure load. He later made diagrams for different pile dimension, soil strength profiles and different loading inclinations.

Generally the shape of the failure envelop under combined loads yields to the function

$$\left(\frac{H}{H_u}\right)^a + \left(\frac{V}{V_u}\right)^b = 1 \qquad (8)$$

where H_u and V_u are the pure ultimate horizontal and vertical loading capacity under pure horizontal translation and vertical translation failure mode (Randolph, Cassidy, Gourvenec, & Erbrich, 2005). The value of a and b have been both proposed to be 3 (Senders & Kay, 2002), but Supachawarote et al. (2005) suggested different expressions of a and b as a function of pile dimension, according to his study using finite element analysis:

$$a = \frac{L}{D} + 0.5 \qquad (9)$$

$$b = \frac{L}{3D} + 4.5 \qquad (10)$$

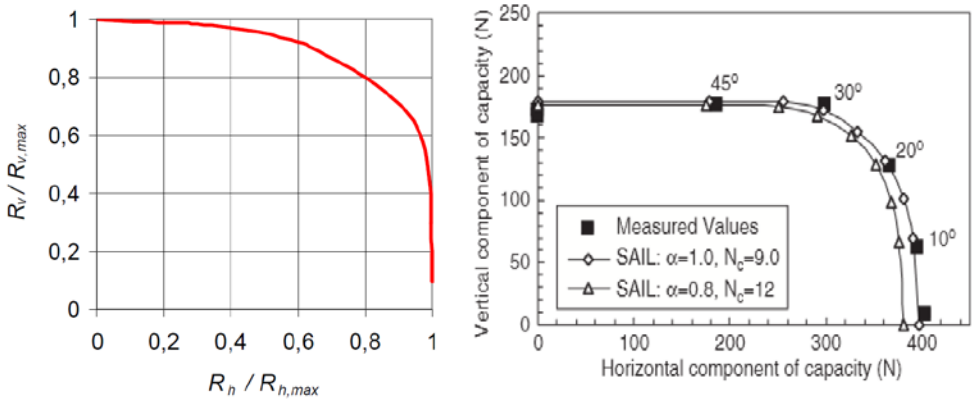

(a) (b)

Figure 12 Coupling between vertical and horizontal loading capacity: (a) extracted from DNV (2005), (b) extracted from EL-Sherbiny et al. (2005).

3.3.3 Specific case

Based on the background given above, the loading capacity largely depends on various factors such as load position, load angle, failure mechanism, vertical/horizontal capacity combination, set-up effect, soil profile (one layer or multi-layer) etc., hence this thesis project requires several specific assumptions and simplifications:

1. The load attachment point is assumed at the optimal load position where translational failure mode occurs without rotation. The exact location is taken as 70 percent of the caisson embedment depth, see Figure 8.
2. Assume that the mooring cable stays horizontally at the lower end (padeye) when considering no current effect. When tidal current poses loading effect, the cable tends to move and thus leading to a loading angle to horizontal at the padeye, but the angle is likely to be very small due to the long length (1000-2000 m) of cable line, so it is likely that the horizontal loading capacity dominates. Therefore in this project, the loading inclination is simplified to horizontal and the failure is governed by lateral loading capacity only. For non-horizontal loading inclination or complex loading combinations, advanced methods discussed in Chapter 3.3.1.3 should be considered.
3. Soils considered in this project only include normally consolidated clay and uniform clay. Normally consolidated soil has a shear strength profile that increases along soil depth, and oppositely uniform soil owns uniform shear strength along depth, see Figure 13. Complex stress paths are not considered.
4. Although FEM remains the most favorable design method from the standpoint of calculation accuracy and similitude with reality, the design will mostly follow the easy-to-use loading capacity factor method initiated by Broms (1964) and Matlock (1970) and later recommended by API (2005). The ultimate resistance is taken as distributed resistance along the anchor-soil interface. It also means that the determination of bearing capacity is based on empirical method without taking

into account the exact failure mode.

5. Ultimate design load on caissons has been calculated in Chapter 3.2, and when considering ultimate limit state design, it is regarded as collapse load equivalent with ultimate soil resistance. Based upon empirical method predicting bearing capacity of a given suction caisson, the caisson dimension is computed through iteration until the ultimate resistance reaches the ultimate design load initiated in Chapter 3.2.

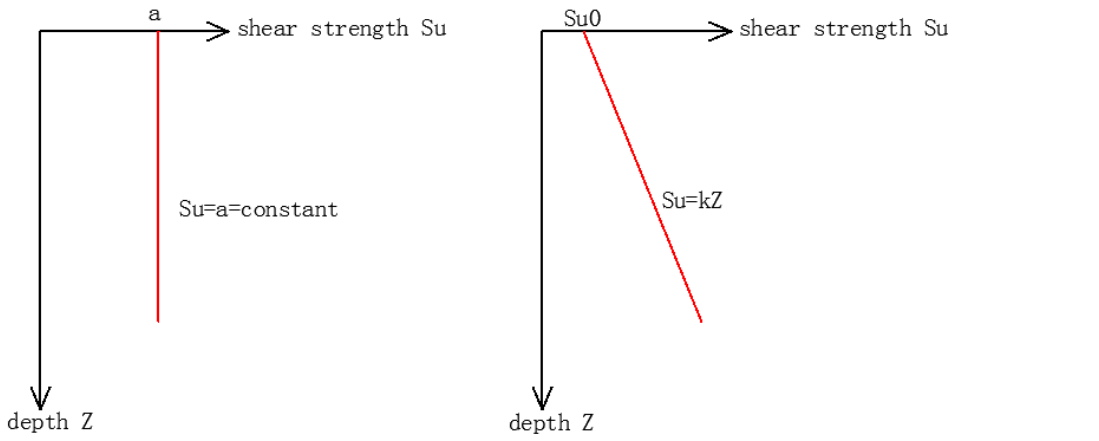

(a) Uniform clay strength profile (b) Normally consolidated clay strength profile

Figure 13 - Undrained shear strength profile of clay

The ultimate unit soil resistance P_u, is computed by equation 14

$$P_u = N_p S_u D \tag{11}$$

Loading capacity factor N_p increases from 3 to 9 as depth Z increases from soil surface to a certain depth Z_R (API, 2005):

$$N_p = 3S_u + \gamma Z + JS_u Z/D \text{ for } Z < Z_R \tag{12}$$

$$N_p = 9 \text{ for } Z \geq Z_R \tag{13}$$

Where γ = effective unit soil weight, here value of 20kN/m^2 is taken;

J = dimensionless empirical constant with value varying from 0.25 for soft clay to 0.5 for stiff caly. In this project due to the absence of soil data, J is set to 0.4;

Z_R = the depth of reduced resistance, m.

Considering a pile diameter D, for a pile segment with vertical length ΔZ the ultimate resisting forces

$$\Delta F = P_u \Delta Z \tag{14}$$

according to Broms (1964) and Aubedy & Murff (2005).

3.4 Results for uniform clay

For uniform clay where the undrained shear strength S_u stays constant over depth (Figure 13-a), the depth of reduced resistance Z_R can be obtained through equaling Equation 15 to Equation 16:

$$Z_R = 6D/(J + \gamma D/S_u) \tag{15}$$

As can be seen from Figure 14

$$P_u = (3 + 6Z/Z_R)S_u D \text{ at } Z < Z_R \tag{16}$$

$$P_u = 9S_u D \; at \; Z > Z_R \tag{17}$$

The loading capacity R_u is then computed by integrating P_u along the pile length, and the integration can be made over a shallow depth where $Z < Z_R$ and a deep depth where $Z > Z_R$. Therefore

$$R_{shallow} = \int_0^{Z_R} N_p S_u D dZ = 6S_u D Z_R \tag{18}$$

$$R_{deep} = 9S_u D(L - Z_R) \tag{19}$$

$$R_u = R_{shallow} + R_{deep} \tag{20}$$

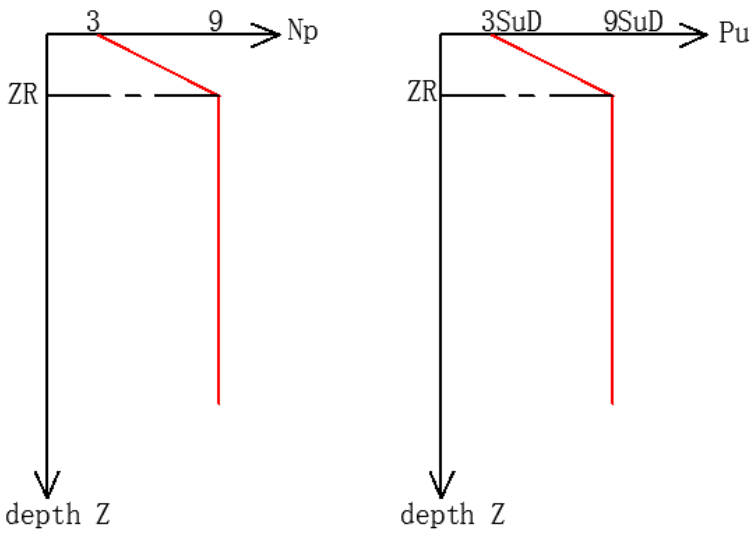

Figure 14 – Lateral resistance of uniform clay

From Chapter 3.2, design lateral loading on each suction anchor has been calculated under various combinations of cable top angle and current event. In addition to that, given the uniform soil shear strength, one can easily obtain the combination of pile diameter and length by prescribing one values of them. A series of combination of pile dimension and length is made, see Appendix B. The results are presented for various soil shear strength and various loading conditions in Figure 15-17.

The design leads to reasonable results. Firstly, for the same soil strength and caisson diameter, caisson length is always required longer for stronger current event; when soil strength increases the required caisson length will correspondingly decrease, if keeping environmental loading and caisson diameter constant; along with larger pile diameter is the reduction of caisson length, providing loading conditions and soil strength maintained constant. It can be seen that aspect ratio L/D remains constant at high undrained shear strength, especially for large diameter caissons. The reason may be that at high soil strength, the pile is relatively short and the resistance provided by the upper soil above critical depth Z_R takes a large proportion of the total resistance. Furthermore, along with increasing soil strength, the critical depth Z_R will increase (Equation 18) leading to a more slowly varying N_p (bearing capacity factor) distribution over depth, hence the required caisson length may reduce little, or even increase in some cases.

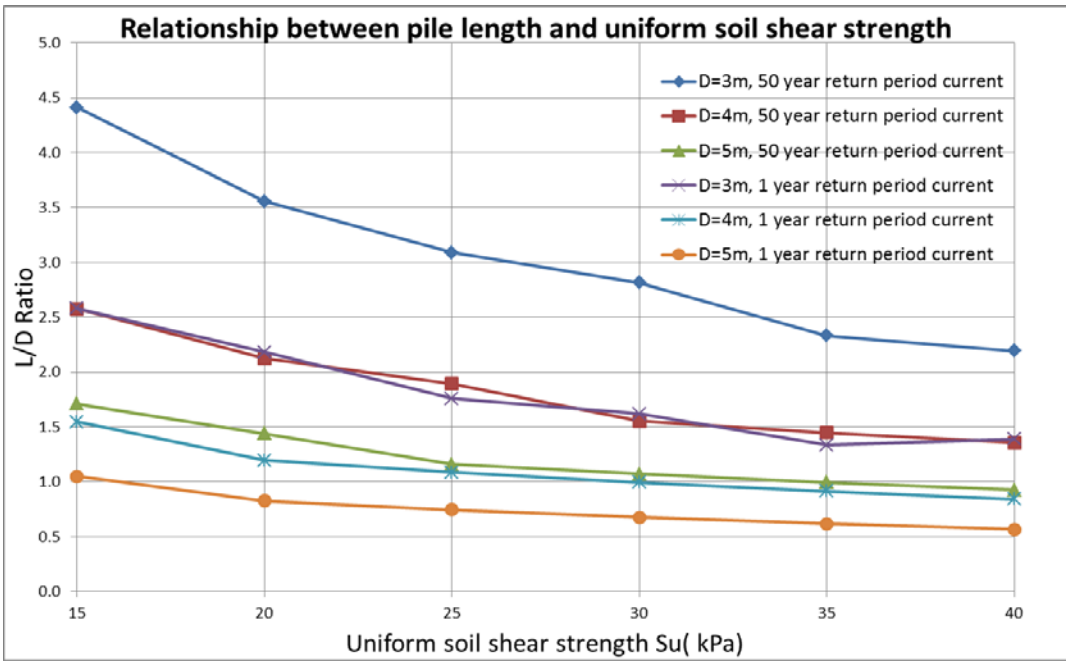

Figure 15 - Pile length for uniform soil under 50 and 1 year return period current event when the cable is 71 degree to horizontal at the top end

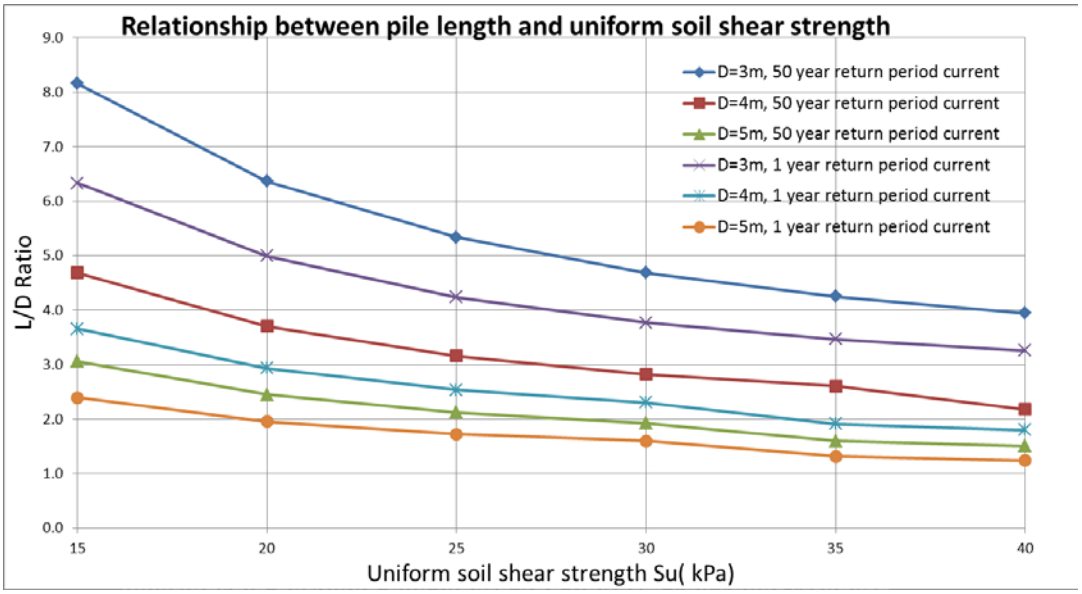

Figure 16 - Pile length for uniform soil under 50 and 1 year return period current event when the cable is 45 degree to horizontal at the top end

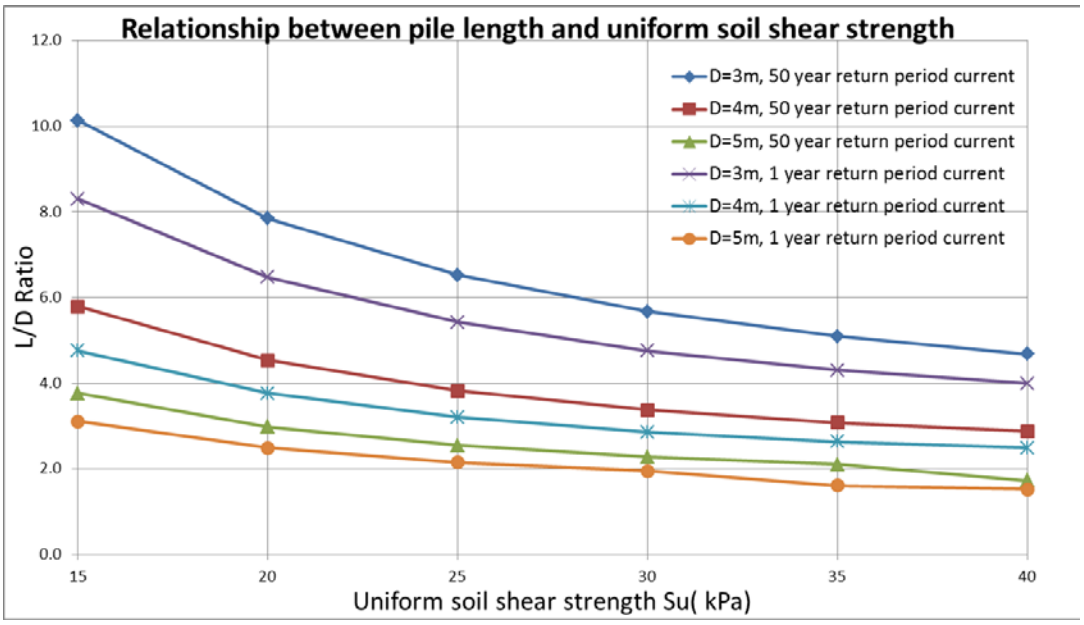

Figure 17 - Pile length for uniform soil under 50 and 1 year return period current event when the cable is 37 degree to horizontal at the top end

3.5 Results for normally consolidated clay

For normally consolidated clay where undrained shear strength Su varies linearly along depth (Figure 13-b), i.e.,

$$S_u = S_{u0} + kZ \tag{21}$$

The depth of reduced resistance Z_R can be obtained by iteratively solving equation 25 (API, 2005):

$$3S_u + \gamma Z + JS_u Z/D = 9 \tag{22}$$

As can be seen from Figure 18,

$$P_u = D\left[\frac{6k}{Z_R}Z^2 + \left(3k + \frac{6S_{u0}}{Z_R}\right)Z + 3S_{u0}\right] \; at \; Z < Z_R \tag{23}$$

$$P_u = 9D(S_{uo} + kZ) \; at \; Z > Z_R \tag{24}$$

The loading capacity R_u is then computed by integrating P_u along the pile depth, and the integration can be divided into two parts: $R_{shallow}$ which is intgrated on shallow depth where $Z < Z_R$ and R_{deep} which is integrated on deep depth where $Z > Z_R$. Therefore

$$R_{shallow} = \int_0^{Z_R} N_p S_u D dZ$$
$$= \frac{1}{3} J k {Z_R}^3 + \left(\frac{3}{2} Dk + \frac{1}{2}\gamma D + \frac{1}{2} J S_{u0}\right) {Z_R}^2 + 3 D S_{u0} Z_R \quad (25)$$

$$R_{deep} = \frac{9}{2} D(2S_{u0} + kZ_R + kL) \quad (26)$$

From Chapter 3.2, design lateral loading on each suction anchor has been calculated under various combinations of cable top angle, soil profile and current event. Given the soil shear strength parameters S_{u0} and k, treating the calculated load as the ultimate lateral load, one can easily get the combination of pile diameter and length by prescribing one values of them. A series of combination of pile dimension and length is made, see Appendix C. The results are graphed under various soil shear strength and various loading conditions, see Figure 19-21.

In normally consolidated clay, the required caisson length against other parameters such as soil strength parameters, caisson diameter and lateral loadings almost follows the same trend displayed in uniform clay, see Chapter 3.3.3.1.

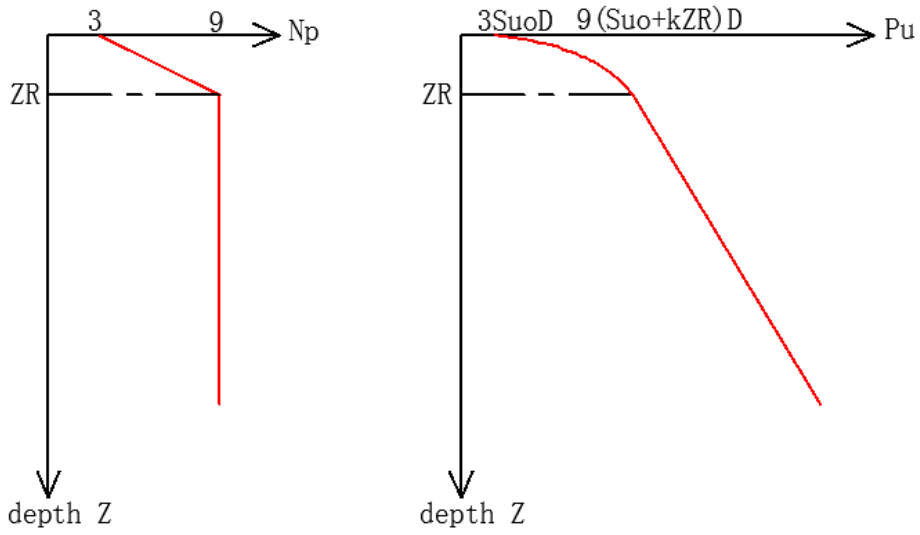

Figure 18 - Lateral resistance of normally consolidated Clay

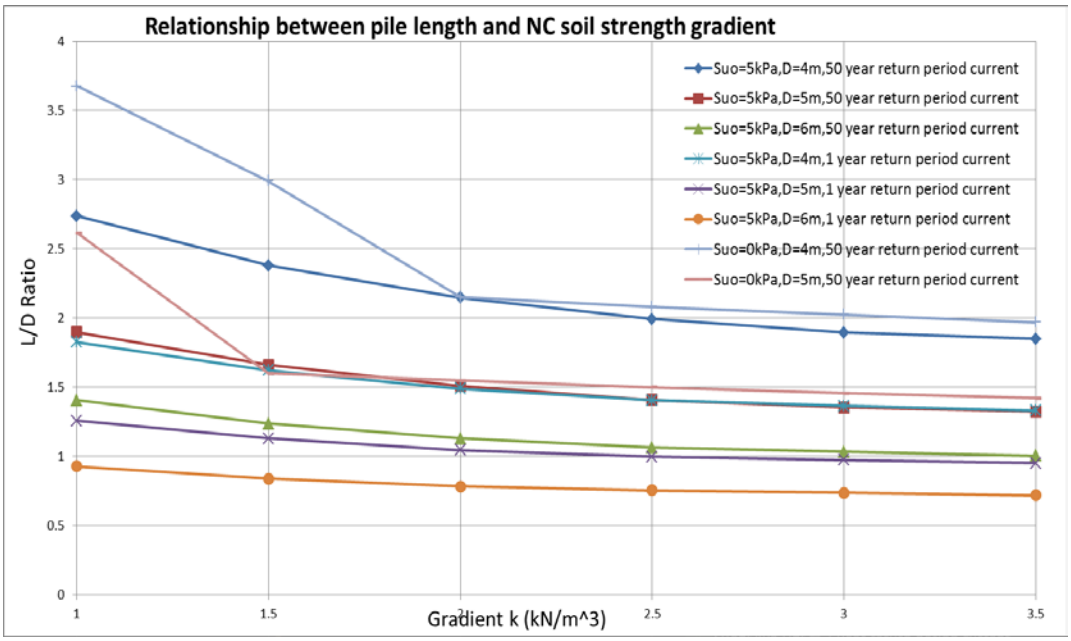

Figure 19 - Pile length for normally consolidated soil under 50 and 1 year return period current event when the cable is 71 degree to horizontal at the top end

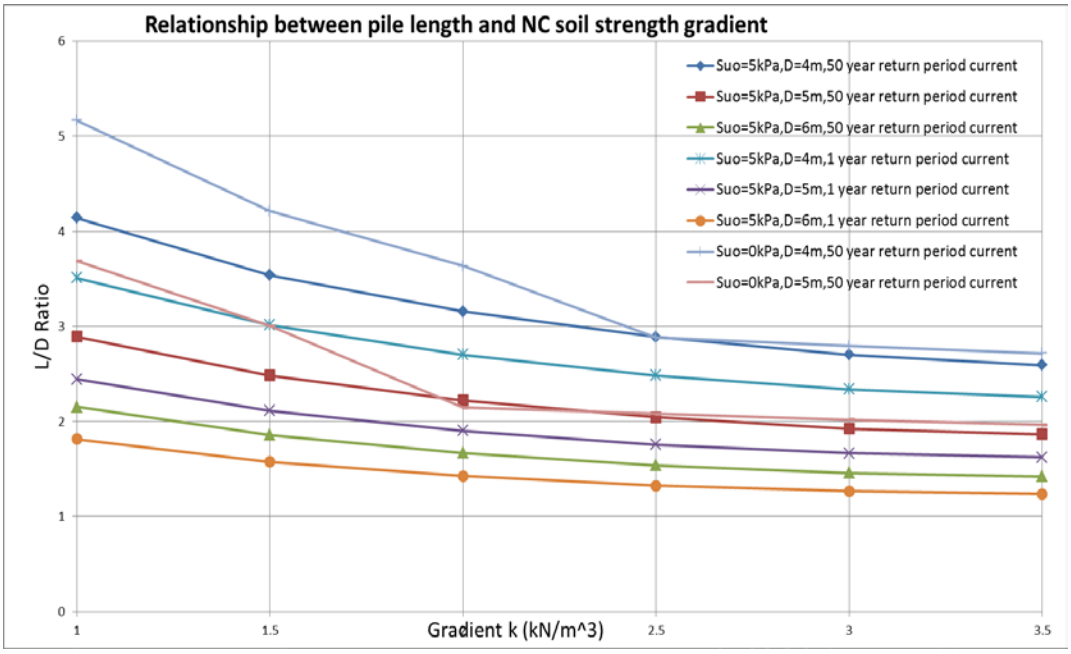

Figure 20 - Pile length for normally consolidated soil under 50 and 1 year return period current event when the cable is 45 degree to horizontal at the top end

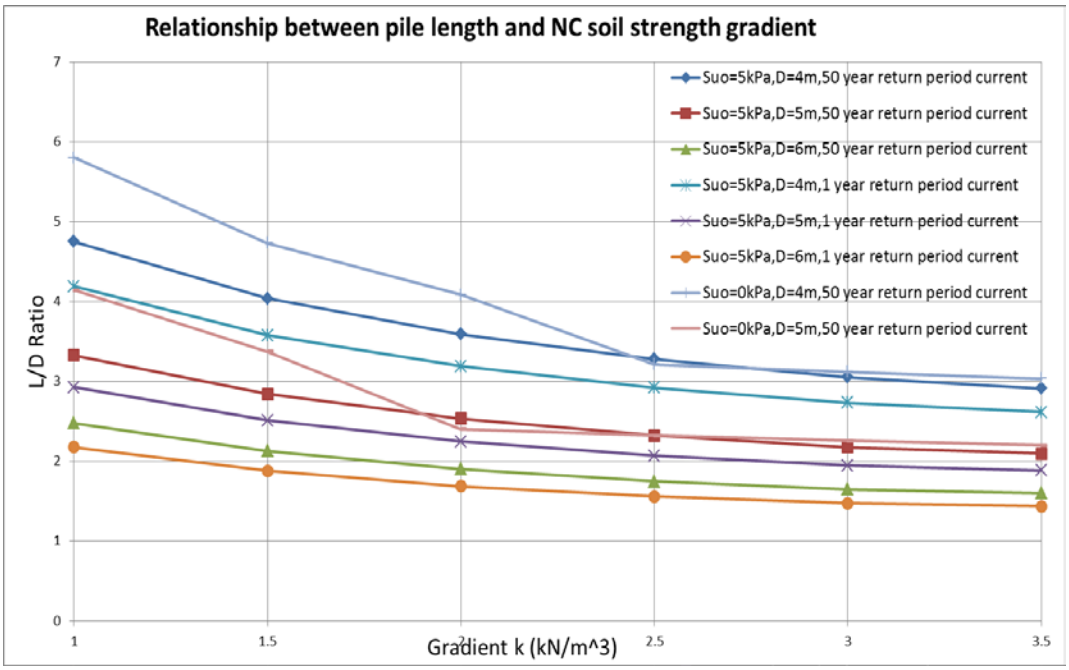

Figure 21 - Pile length for normally consolidated soil under 50 and 1 year return period current event when the cable is 37 degree to horizontal at the top end

4 Pile deflection analysis

4.1 General

In addition to considerations from the standpoint of ultimate limit state, deformation level, also termed serviceability limit state (SLS), should fulfil corresponding requirements (DNV, 2005), hence the load-displacement response of laterally loaded pile is of significance. In general, the soil around a laterally loaded pile behaves as plastic material therefore the relationship between pile deflection and soil resistance shows non-linear response, which makes it necessary to plot the lateral resistance on a unit length of the pile *p* against pile deflection *y* at that depth, namely *p*-*y* curve (Matlock, 1970; Murff & Hamilton, 1993; API, 2005).

The *p*-*y* curve method is primarily proposed by Matlock (1970) who analysed the pile-soil interaction problem by considering pile-soil system as a complex beam-column foundation. He divided the pile into segments and separated the soils into a series of layers surrounding the pile segments. These soil layers are considered as independent non-linear springs with different properties, which provide the resistance *p* corresponding to the pile-soil deflection *y* at every depth, see Figure 22.

Based on a number of field tests on instrumented laterally loaded piles, laboratory experimental tests as well as analytical study under various static and cyclic lateral loading conditions, many different versions of *p*-*y* curve have been constructed and recommended for various conditions, e.g., soft clay, above water table stiff clay criteria, below water table stiff clay criteria, API recommendation, unified clay criteria, integrated clay criteria, p-y Curve based on Bezier Equations. See details on paper of Pradhan (2012).

Among all these models, the API recommendation has been most widely adopted by geotechnical engineers around the world (Chakrabarti, 2005; Pradhan, 2012). It is based on the work done by Matlock (1970) and Reese et al. (1975) and it is the only method that is fully described within a standard code. For soft clay, the *p*-*y* curve under short-term static loading is expressed as below (see Figure 23):

$$\frac{P}{P_u} = 0.5\left(\frac{y}{y_c}\right)^{\frac{1}{3}} \tag{27}$$

Where P = the actual lateral resistance, kPa;

y = the actual lateral deflection, m;

$y_c = 2.5\epsilon_{50}D$, m;

ϵ_{50} = strain which occurs at one half the maximum stress on laboratory unconsolidated undrained compression tests of undisturbed soil samples.

The *p*-*y* curve can also be generated from Table 7 (API, 2005)

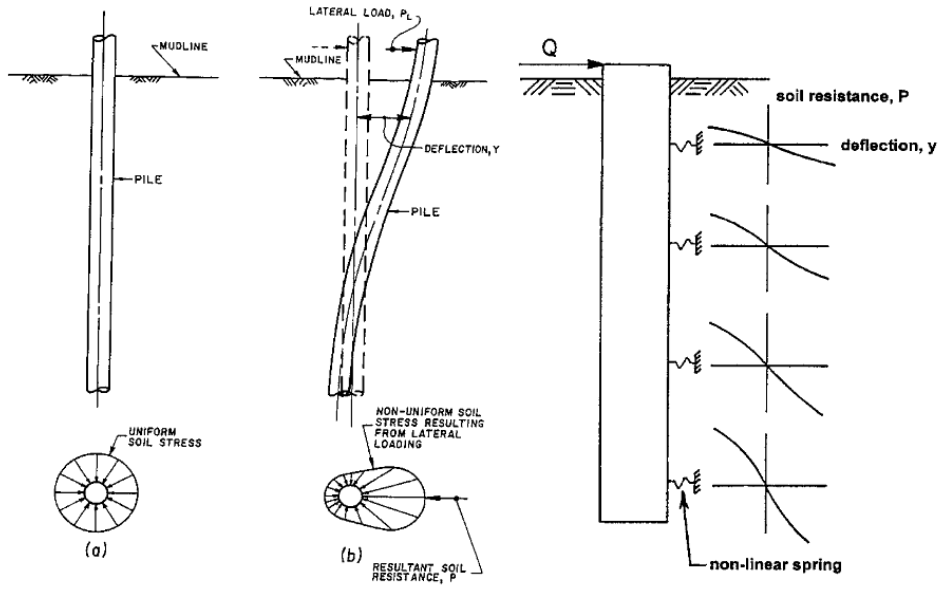

Figure 22 - Lateral Soil Resistance - Pile Deflection (*p-y*) Analysis Given by Chakrabarti, 2005

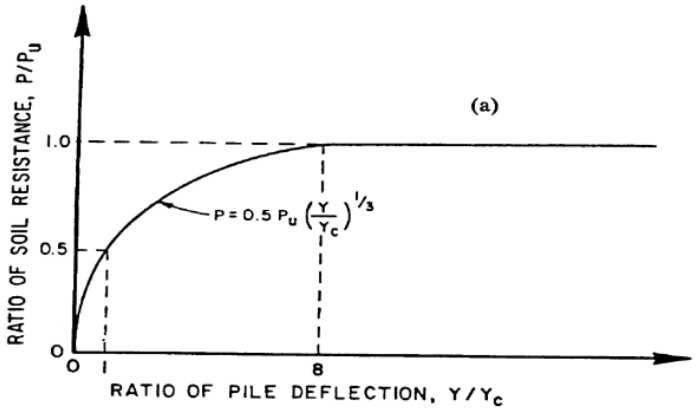

Figure 23 - *p-y* Curve for Soft Clay under Static Loading Given by API, 2005

Table 7 – *p-y* Curve Data for Short-Term Static Load for Soft Clay, from API, 2005

p/p_u	y/y_c
0.00	0.0
0.23	0.1
0.33	0.3
0.5	1.0
0.72	3.0
1.00	8.0
1.00	∞

4.2 Specific case-short-term static loading condition

This chapter will deal with the pile-soil interaction. Some specifications have to be made before doing the analysis:

1. The optimal load attachment point (70% of caisson embedment depth) as well as the almost horizontal load inclination guarantees that, the suction caisson is under horizontal translation without rotation neither vertical movement.
2. As can been seen from the design, the suction caisson aspect ratio ***L/D*** is generally small. It is further assumed that the suction caisson has very high stiffness so that it can be regarded as a rigid body.
3. Based on the above two simplifications, the suction pile is subjected to rigid lateral movement, meaning that the pile-soil deflection is totally horizontal and keeps the same value along anchor depth, i.e., deflection ***y*** remains constant over depth.
4. The strain ϵ_{50} corresponding to half the maximum unit lateral resistance typically falls with the range from 0.005 to 0.02 according to Matlock (1970), with the smaller value applicable to sensitive or brittle clay while the larger value to remodeled or disturbed or unconsolidated sediments. In this case choose $\epsilon_{50} = 0.008$ so that

$$y_c = 2.5\epsilon_{50}D = 0.02D \tag{28}$$

Therefore for a specific pile, y_c and y remains constant along anchor depth, and according to Equation 30, P/P_u will stay constant at different depth. I.e., the real unit lateral resistance distribution along the anchor length follows the profile of ultimate unit lateral resistance distribution, but with a constant reduction factor. The reduction of unit lateral resistance can be computed through the reduction of the load at padeye, i.e.,

$$\frac{F}{R_u} = \frac{\int_0^L p dZ}{\int_0^L p_u dZ} = \frac{p}{p_u} \tag{29}$$

Where R_u= lateral loading capacity calculated in Chapter 3.2.

Hence the relationship between load at padeye and pile lateral translation can be established as

$$\frac{F}{R_u} = 0.5\left(\frac{y}{y_c}\right)^{1/3} \tag{30}$$

4.3 Results

The relationship between F and y can be easily computed and graphed in an excel spread sheet, providing the pile dimension and the soil strength profile. Example of the $F - y$ curve construction on excel sheet spread have been attached in Appendix D. The results of pile-soil behaviour under various conditions have been plotted such as: behaviour at different pile dimensions designed for the same loading capacity; behaviour at various piles lengths; behaviour at various soil strength profiles, see Figure 24-29.

From Figure 24 and Figure 27, it can been seen that for the same soil strength and the same bearing capacity, when the caisson has smaller diameter and longer length, deflection becomes less under the same load, meaning that soil behaviour stiffer. Figure 25 and Figure 28 show that shorter piles have larger stiffness, providing the soil strength and pile diameter constant. Also Figure 26 and Figure 29 indicate that generally larger soil strength guarantees stronger stiffness. All the figures also show that the horizontal displacement at ultimate load remains quite large, with maximum value reaching 1.0 meter.

Since the calculated horizontal translation stands for short-term static response of the caisson, it is expected worse in terms of deformation under long-term dynamic environmental conditions, as explained by (Andersen, 2009). Therefore refined design method is highly recommended to satisfy serviceability requirement.

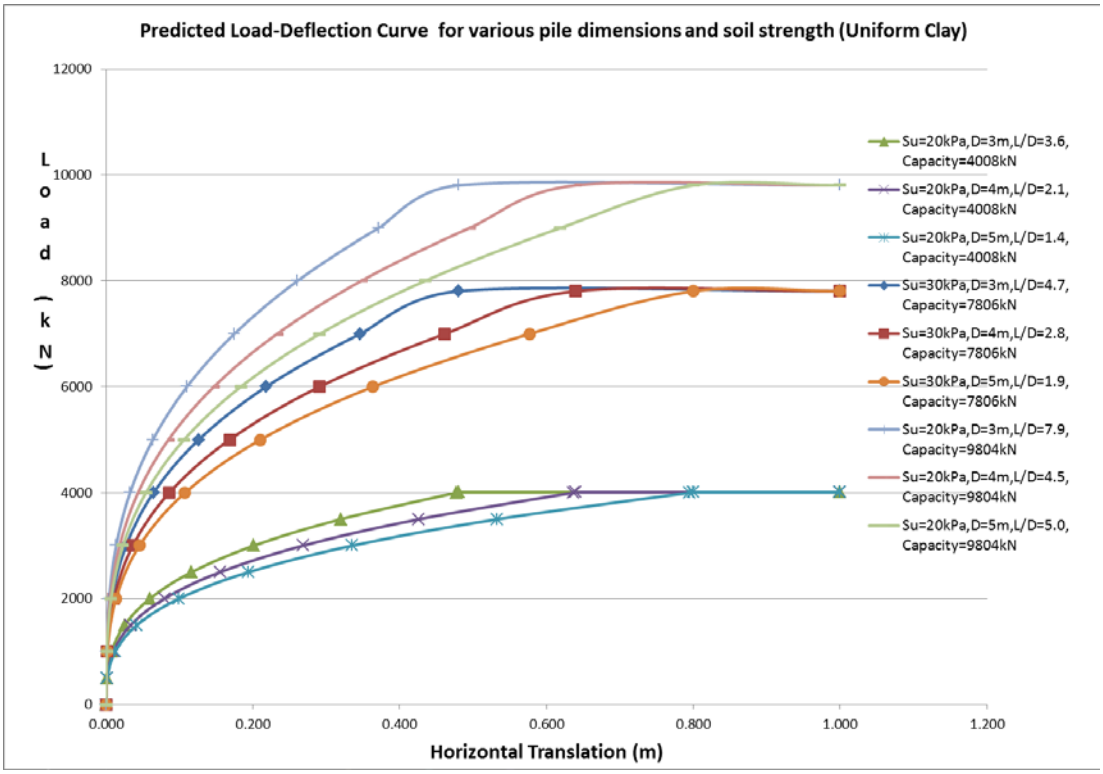

Figure 24 - Predicted load-deflection curve for various uniform clay and pile dimensions

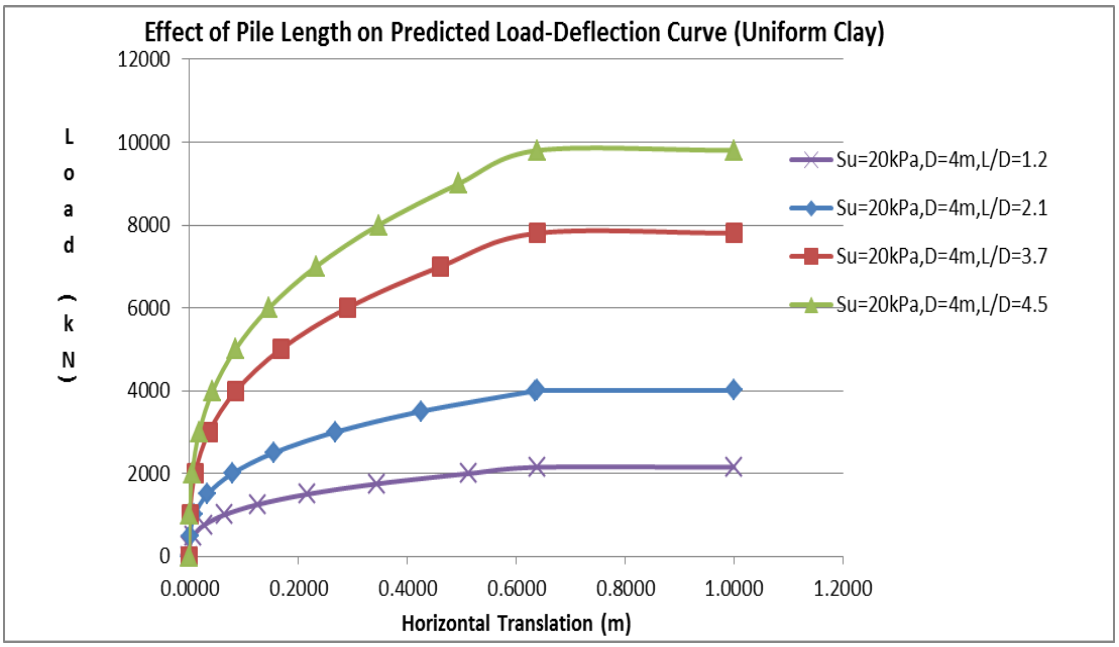

Figure 25 - Effect of L/D ratio on predicted load-deflection curve for uniform clay

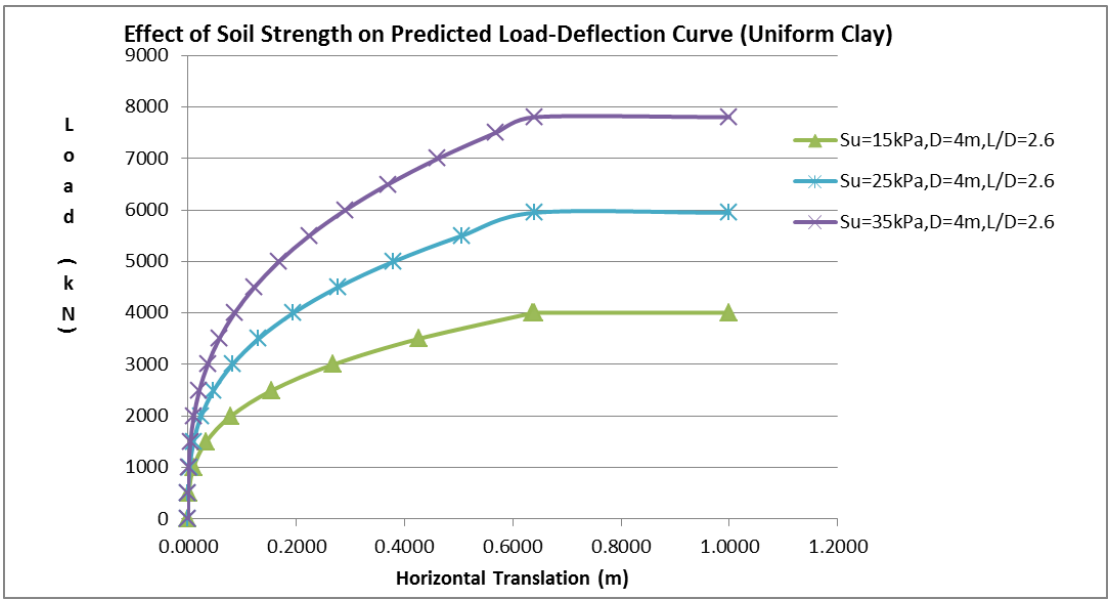

Figure 26 - Effect of soil strength on predicted load-deflection curve for uniform clay

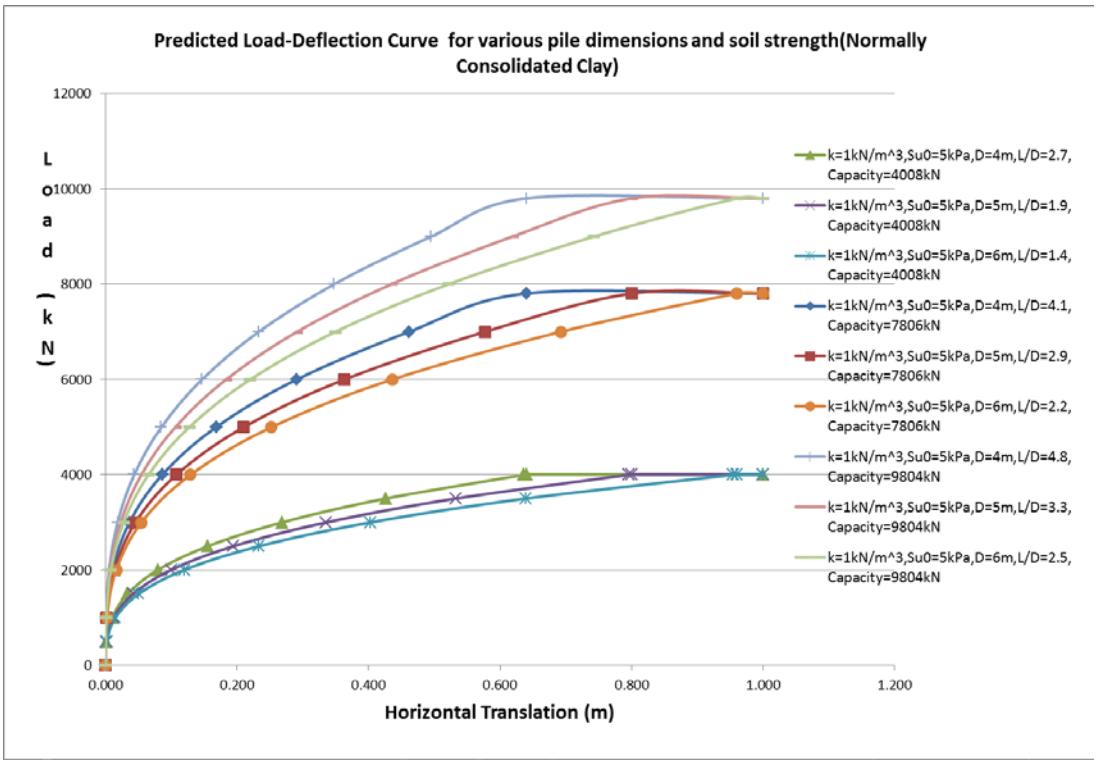

Figure 27 - Predicted load-deflection curve for various normally consolidated clay, and pile dimensions

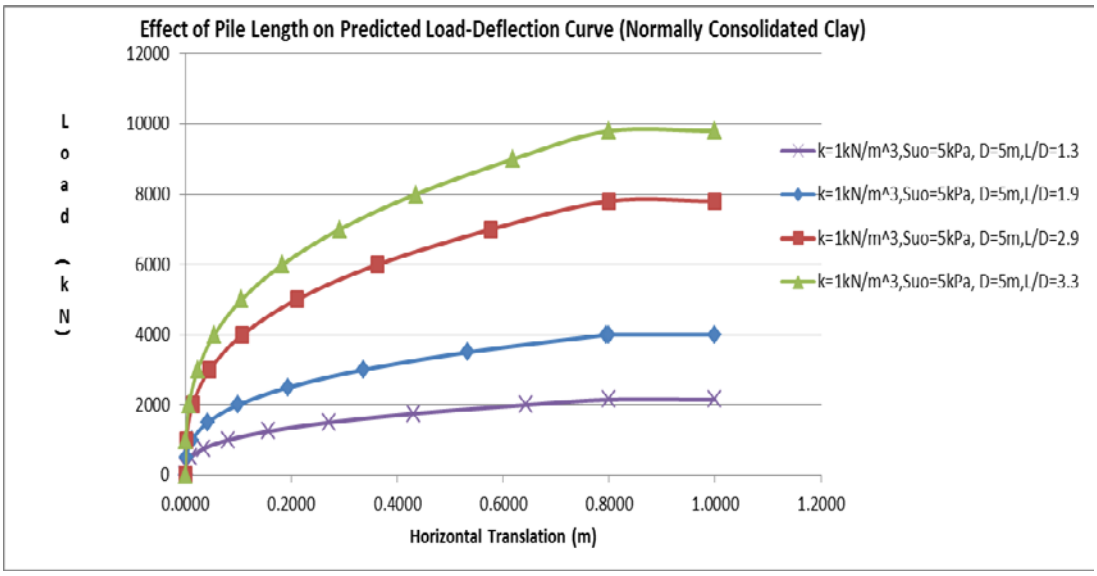

Figure 28 - Effect of pile length or L/D ratio on predicted load-deflection curve for normally consolidated clay

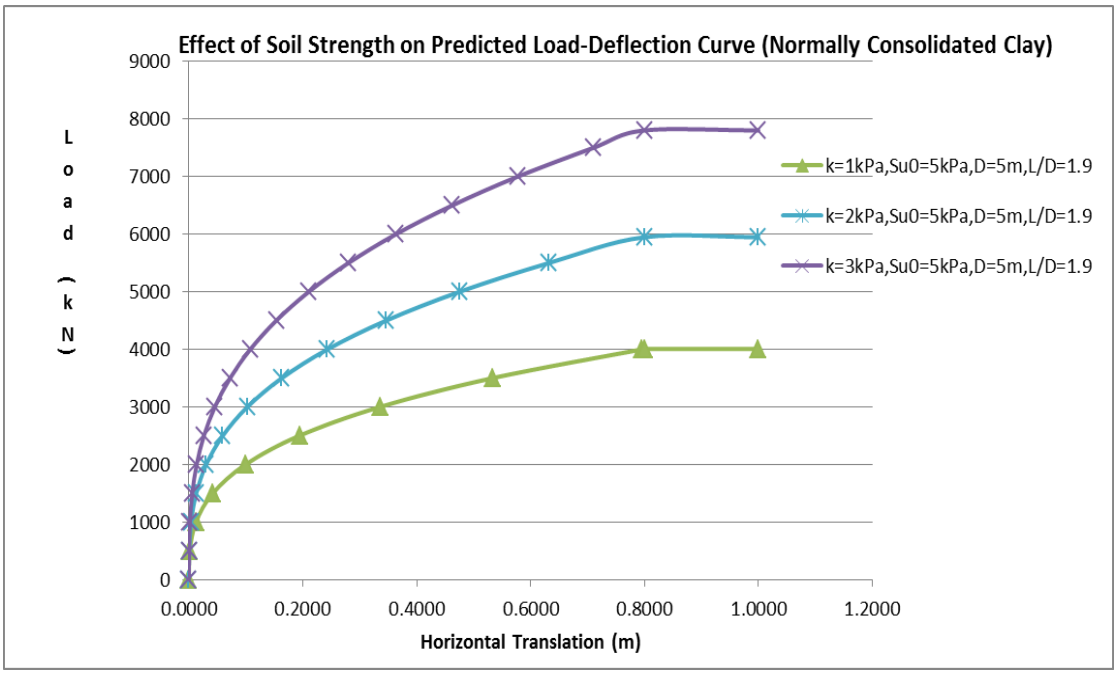

Figure 29 - Effect of soil strength on predicted load-deflection curve for normally consolidated clay

5 Design of laboratory modelling on the effect of cyclic loading on the behaviour of uniform soil around lateral caissons

In Chapter 4 an overview of soil-pile interaction has been displayed under static loading conditions, but since the suction caissons in reality will be subjected to cyclic loads, it has been broadly realized crucial to understand the cyclic behaviour of soil around a suction caisson.

Anderson (2009) systematically described the soil behaviour under cyclic loading, and he pointed out that with increasing number of cycles displacements will increase, and that the displacements become larger than that caused by static loading at the same load value, see Figure 30. He also shows that cyclic bearing capacity is often smaller than static bearing capacity because under cyclic loading condition, the pore water pressure cannot completely dissipate within each cycle which leads to pore pressure accumulation as well as effective stress reduction and therefore soil strength drop accordingly after each cycle, see Figure 31. Soil cyclic shear strength strongly depends on stress path and it shows different characteristics for various combinations of mean shear stress and cyclic stress, and also for various shearing types of the soil element, i.e., direct shearing or triaxial shearing. Therefore cyclic shear strength may be higher than static shear strength for a few loading cycles under some occasions, due to the fact that cyclic shear strength of clay is rate dependent.

While Andersen (2009) directly focused on cyclic behaviour of soil element, many researchers started modelling in laboratory the load-displacement behaviour of pile and obtained soil reaction stiffness properties in laboratory under combined cyclic loading tests both on sand and clay (Kelly, Houlsby, & Byrne, 2006; LeBlanc, Houlsby, & Byrne, 2009; Zhu, Byrne, & Houlsby, 2012). Kelly et al. (2006) derived dimensionless scaling equations for piles in sand and clay, which benefits comparing laboratory and field tests. The equations are derived from assumed elastic force-displacement relations, i.e., elastic stiffness, and reaches dimensionless relations between loads and displacement, e.g., moment-rotation relation, vertical load-vertical displacement relation. Based mainly upon the non-dimensional equations, Kelly et al.(2006) conducted physical experiments on sand and clay in laboratory as well as in field, and he compared moment stiffness and vertical stiffness under cyclic moment loading and vertical loading respectively both in sand and clay. Later Leblanc et al. (2009) and Zhu et al.(2012) based on the dimensionless equations proposed by Kelly et al. (2006) made also laboratory work under cyclic loading on sand and found that moment stiffness may increase with number of cycles (LeBlanc, Houlsby, & Byrne, 2009) or stay constant with accumulated rotation (Zhu, Byrne, & Houlsby, 2012).

Through the efforts made by these authors, mainly moment stiffness for sand are investigated, but less attention is paid to the relation between lateral load and lateral displacement of suction caisson in clay, which is the case in this thesis project. Also, the dimensionless equations proposed by Kelly et al. (2006), Leblanc et al. (2009) and Zhu et al.(2012) initially depend on elastic stiffness matrix (see Equation 34), but for this case lateral loading – lateral displacement correlations are assumed non-linear at least under static loadings, as can be seen from Equation 33.

Therefore this chapter will design physical modelling tests of suction caisson in clay to investigate the soil behaviour, e.g., development of soil stiffness under cyclic lateral loading. The results will be properly scaled to predict the full-scale behaviour of suction caisson designed in Chapter 4 and to verify the fundamental p-y curve method.

$$\begin{bmatrix} V \\ M/D \\ H \end{bmatrix} = DG \begin{bmatrix} k_1 & 0 & 0 \\ 0 & k_3 & k_4 \\ 0 & k_4 & k_2 \end{bmatrix} \begin{bmatrix} w \\ D\theta \\ u \end{bmatrix} \quad (31)$$

where G is the soil shear modulus, w, $D\theta$ and u are vertical, rotational and horizontal displacements, and k_1, k_2, k_3 are dimensionless elastic constants

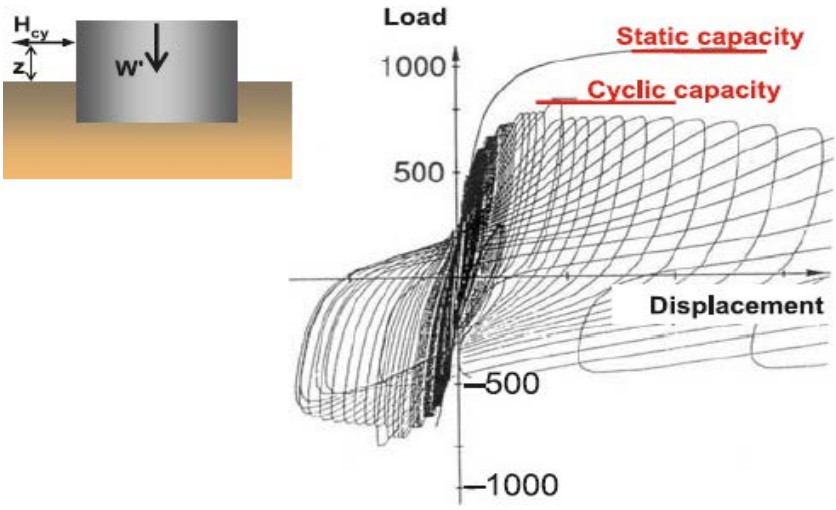

Figure 30 - Test on static and cyclic loading on gravity platform on clay (Andersen 2009)

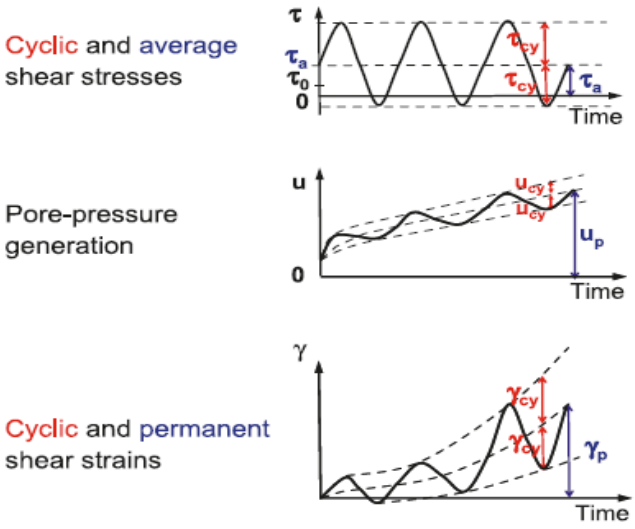

Figure 31 -Pore water pressure and shear strain accumulation over loading cycles under undrained condition (Andersen, 2009)

5.1 Dimensionless equations for comparison of laboratory and full-scale field tests on uniform clay

Laboratory physical modelling is often performed to investigate specific behaviour of prototype in controlled conditions, and since most modelling is usually conducted in a smaller scale compared with prototype, it is necessary to know how the results derived from physical modelling can be interpreted to predict the behaviour of the full-scale prototype (Muir Wood, 2004). Typically dimensionless analysis is performed to build up relations between dimensionless parameters and thus providing proper scale factors linking laboratory and prototype tests (Kelly, Houlsby, & Byrne, 2006).

Kelly et al (2006) derived dimensionless equations reflecting linear behaviour of soil, but in this thesis dimensionless equation will be derived, based upon non-linear behaviour of soil, from Equation 33 for static lateral load-displacement characteristics:

$$\frac{F}{R_u} = 0.5\left(\frac{y}{y_c}\right)^{1/3}$$

It is known that ultimate resistance R_u depends on undrained shear strength of clay, and for a suction caisson with constant crossing area installed in uniform clay, it satisfies

$$R_u = \int_0^L P_u dz = \int_0^L N_p S_u D dz = \overline{N_P} S_u D L \tag{32}$$

In particular,

$$R_u = (9 - 3\,Z_R/L) S_u D L$$

$$R_u = (3 + 3\frac{1}{Z_R/L}) S_u D L \tag{33}$$

for long caissons ($L > Z_R$) and short caissons ($L < Z_R$) respectively.

According to Equation 18,

$$Z_R = 6D/(J + \gamma D/S_u)$$

Therefore

$$\frac{Z_R}{L} = 6\frac{D}{L}\frac{1}{(J + \gamma D/S_u)} \tag{34}$$

On the other hand, the value of y_c is proportional to $\epsilon_{50} D$. The value of ϵ_{50} may be higher in prototype soil than in laboratory sample since soil stiffness *G* is larger in prototype due to the higher vertical effective stress (LeBlanc, Houlsby, & Byrne,

2009), but for most clays it falls into the range between 0.005 to 0.02 (Matlock, 1970) so it is taken the same value of 0.008 for prototype and laboratory soil.

Substitute Equation 31, 36 and 37 into Equation 33 to obtain

$$F = \frac{0.5}{0.02^{1/3}}(9 - 18\frac{D}{L}\frac{1}{(J + \gamma D/S_u)})S_u DL\left(\frac{y}{D}\right)^{1/3}$$

$$F = \frac{0.5}{0.02^{\frac{1}{3}}}(3 + \frac{L}{2D}(J + \frac{\gamma D}{S_u}))S_u DL\left(\frac{y}{D}\right)^{1/3} \quad (35)$$

for long caissons $(L > Z_R)$ and short caissons $(L < Z_R)$ respectively.

Obtain dimensionless equation by dividing Equation 38 by $S_u D^2$

$$\frac{F}{S_u D^2} = \frac{0.5}{0.02^{1/3}}(9 - 18\frac{D}{L}\frac{1}{(J + \gamma D/S_u)})\frac{L}{D}\left(\frac{y}{D}\right)^{1/3}$$

$$\frac{F}{S_u D^2} = \frac{0.5}{0.02^{\frac{1}{3}}}(3 + \frac{L}{2D}(J + \frac{\gamma D}{S_u}))\frac{L}{D}\left(\frac{y}{D}\right)^{1/3} \quad (36)$$

Rewrite as

$$\tilde{F} = \tilde{k}\tilde{y}^{1/3} \quad (37)$$

where

$$\tilde{F} = \frac{F}{S_u D^2}$$

$$\tilde{k} = f\left(\frac{L}{D}, \frac{\gamma D}{S_u}\right) = \frac{0.5}{0.02^{1/3}}(9 - 18\frac{D}{L}\frac{1}{(J + \gamma D/S_u)})\frac{L}{D}\ for\ long\ piles\ or$$

$$\tilde{k} = f\left(\frac{L}{D}, \frac{\gamma D}{S_u}\right) = \frac{0.5}{0.02^{\frac{1}{3}}}(3 + \frac{L}{2D}(J + \frac{\gamma D}{S_u}))\frac{L}{D}\ for\ short\ piles$$

$$\tilde{y} = \frac{y}{D}$$

Equation 39 and 40 suggests satisfactory comparison between laboratory and field tests by plotting dimensionless parameters $\tilde{F}$ against $\tilde{y}$ providing that parameters determining the value of $\tilde{k}$, i.e., $\frac{L}{D}, J$ and $\frac{\gamma D}{S_u}$ are the same in laboratory and field tests.

5.2 Scaling of pile dimension, soil strength and consolidation time

Centrifuge test is becoming popular in geotechnical modelling for reproducing the real scale stress level, but often very small number of loading cycles can be applied in this kind of test which limits its application on cyclic modelling. Hence centrifuge tests are infeasible due to the large number of loading cycles required in laboratory work and as well as due to the limitation of currently available facilities at Chalmers, so 1g scaled tests are proposed for this project instead.

For a prototype: $S_u = 40\ kPa, D = 3\ m, L = 4.2\ m, \frac{L}{D} = 1.4, r = 15\ \frac{kN}{m^3}$

Choose laboratory parameters to make sure $\tilde{\mathrm{k}} = f\left(\frac{L}{D}, \frac{\gamma D}{S_u}\right)$ keeps the same in laboratory and prototype.

Choose scale factors

$n_L = \frac{1}{10}, n_{S_u} = \frac{1}{10}, n_\gamma = 1$, so in laboratory

$S_u = 4kPa, D = 0.3m, L = 0.42m, \frac{L}{D} = 1.4, r = 15\frac{kN}{m^3}$

To perform similar drainage conditions and consolidation speed as in the field, the loading time for one cycle in the lab is supposed to be much shorter than the pore pressure dissipation time. Considering dimensionless time factor

$$T_v = \frac{C_v t}{H^2} \tag{38}$$

Incorporating the definition of consolidation coefficient C_v, permeability K, and constrained modulus or one-dimensional soil stiffness E_{oed}

$$T_v = \frac{C_v t}{H^2} = \frac{Kt}{m_v \gamma_f H^2} = K\frac{tE_{oed}}{\mu H^2} \tag{39}$$

where μ is viscosity of fluid around soil particles, m_v is the coefficient of volume compressibility.

Taking into account that one-dimensional soil stiffness E_{oed} can be regarded as proportional to undrained shear strength S_u (Kelly, Houlsby, & Byrne, 2006), i.e., $E_{oed} = AS_u$ where A is a constant. Insert into Equation 42,

$$T_v = \frac{C_v t}{H^2} = \frac{Kt}{m_v \gamma_f H^2} = K\frac{tE_{oed}}{\mu H^2} = KA\frac{tS_u}{\mu H^2} \tag{40}$$

To achieve in laboratory the same consolidation status or drainage condition as in prototype, the time scale should be satisfied:

$$n_t = \frac{n_u {n_H}^2}{n_{S_u}} \tag{41}$$

The viscosity of fluid depends on the type of fluid as well as temperature. Along with the increase of temperature the viscosity of one fluid will typically decrease. Within this laboratory test, water with constant temperature of 60℃ is under consideration to model the water temperature, say 4℃, at fjord bottom. In fact, $\mu_{60℃=0.47}, \mu_{4℃=1.54}$ according to the information provided by DDBST (2014) on their website. For the chosen parameters in laboratory, the time scale can be calculated

$$n_t = \frac{n_u {n_H}^2}{n_{S_u}} = \frac{\frac{0.47}{1.54} \times (\frac{1}{10})^2}{1/10} = 1/33 \tag{42}$$

In terms of cyclic loading, the time scale of 1/33 indicates a laboratory loading cycle of 22.6 minutes corresponding to one prototype loading cycle of 12 hours and 25 minutes. The temperature of 60℃ is chosen from the consideration of decreasing water viscosity and further reducing modelling time in the laboratory (decrease n_t), but on the other hand it requires a lot of energy since the experiment will last several months, which makes the experiment a bit uneconomical.

5.3 Clay specimens preparation and consolidation

The soil sample preparation and consolidation process mainly follows the steps proposed by Gue (1984), Santa Maria (1988) and Martin (1994), while the apparatus design originates from the idea of Gue (1984) but with a framework proposed by Foglia (2012).

5.3.1 Consolidation equipment

Compared with that of Gue (1984), this apparatus consists of almost the same functional parts (see details in Gue, 1984) including: a soil container, a reaction/loading frame, two porous plastic filters at the bottom of the soil box and at the surface of the slurry, drainage system at the top and bottom of the soil container and a hydraulic ram applying consolidation loading, as can be seen in Figure 32. But differently, the soil container in this project is simplified to a big well-welded rectangular box made of painted steel, with outer dimension of $1.8\,m \times 1.3\,m \times 1.1\,m$ (length × width × height)and thickness of $0.1\,m$. This kind of soil container performs in a way as a base of the loading frame, so it should be well bolted to the ground to keep the stability of the whole system.

A typical slurry consolidation tank is shown in Figure 32. Note that slurry consolidation tanks are different from slurry preparation tanks. There exist three same tanks for static loading, cyclic loading scenario 1 and cyclic loading scenario 2

respectively. In such way, the static p-y curve equation can be verified through parametric study based on data from static test, and the effect of cyclic loading can be investigated by comparing static test and dynamic tests. Dynamic load combinations can also be compared. The final samples in the three tanks are thought to have quite similar properties such as strength profile and water content, meaning that sample creation is repeatable which has been proved by Gue (1984) in lab. A better solution is to build only one consolidation tank from the perspective of cost, but in that way the three tests will have to be made sequentially in the same box and therefore the modelling time would be much longer.

The holes on the loading platen and at the bottom of soil box control the two directional drainage paths and the plastic discs installed both on the top and bottom work as filters. Consolidation loading, except for the self-weight of slurry, is applied to the soil through a hydraulic ram over a flat loading platen. Plastic hoses are installed on the drainage holes at the soil box bottom, to conduct the drained water out from the bottom to the water surface so that a constant hydraulic head is maintained all the time.

For details of the functions of each part, see the description by Gue (1984), Santa Maria (1988) and Martin (1994).

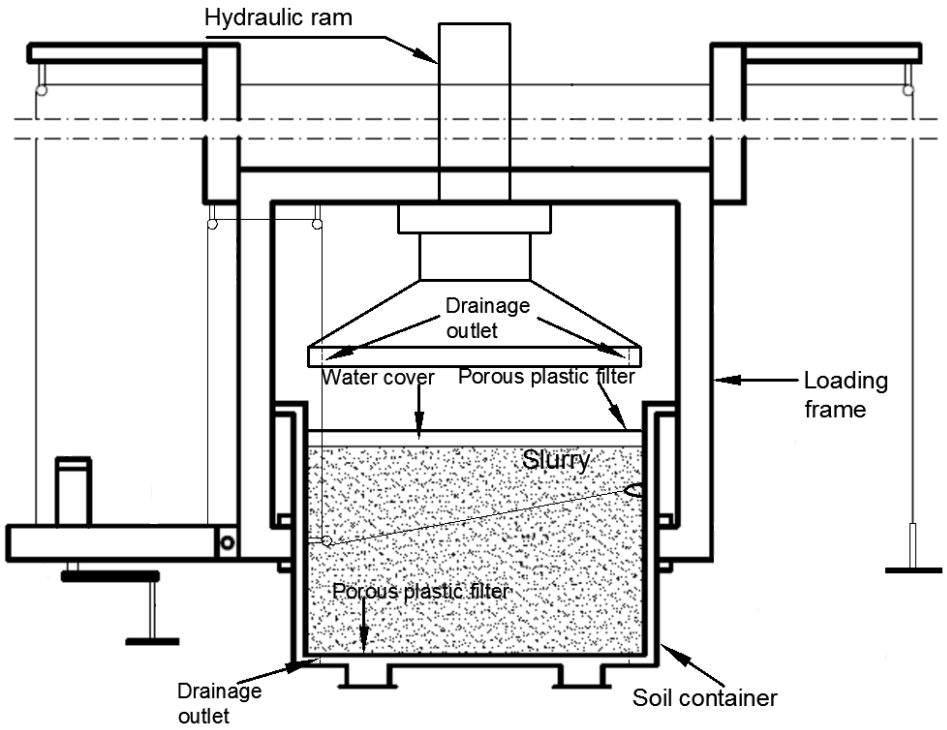

Figure 32 - Sketch of the consolidation apparatus

5.3.2 Kaolin clay

As has been used in many small-scale laboratory experiments, Speswhite Kaolin clay is adopted in this modelling due to its well-known geotechnical properties, including the high permeability benefitting the reconstituted slurry from rapid consolidation (Martin, 1994). Several key parameters of Speswhite Kaolin clay has been

summarised by Martin (1994), e.g., liquid limit $w_l \approx 65\%$, specific solid gravity $G_s \approx 2.61$.

5.3.3 Slurry preparation

The slurry is obtained by mixing Kaolin powder with proper quantity of water for two hours through a mixer mechanically driven by a motor. The quantity of water added is carefully calculated to guarantee initial water content around w=120 %. When mixing Kaolin powder with water, a vacuum of 0.8 bars is applied above the surface of the slurry to get rid of possible air bubbles. The mixed homogeneous slurry is pumped into the three consolidation tanks and then goes through consolidation process under specifically applied loadings. Only one slurry preparation box is needed to mix powder and water.

The final sample depth after consolidation-swelling is desired to be around 0.6 m, based on consideration that the undrained shear strength of clay along the pile needs to be 4 kPa in average to fulfil the governing scaling law, see Appendix E. As observed by Martin (1994) in figure 3-2 of his paper, swelling effect is quite minor compared with the total settlement, therefore the required sample height after complete consolidation under 20 kPa is simplified to be 0.6 m.

It is of significance to calculate the initial slurry height in the consolidation tank to guarantee a final sample height of 0.6 m. Simple calculation lies on one-dimensional consolidation theory providing a proper coefficient of volume compressibility m_v under loading of 20 kPa. Hence it is highly recommended to operate odometer tests of the slurry to obtain the exact value of m_v (and also C_v, coefficient of consolidation), but this project will adopt the value derived from the odometer test results obtained by Santa Maria (1988). Santa Maria (1988) performed odometer tests on slurry similar to that used in this modelling (water content, specific solid gravity), and according to her results (Figure 4.4 and Figure 4.5 in her paper) the coefficient of consolidation and permeability under vertical loading of 20 kPa can be interpolated to be $C_v = 4\ m^2/year$ and $K = 2.0 \times 10^{-8}\ m/s$. Easily one can obtain the coefficient of volume compressibility $m_v = 16.1\ m^2/MN$ according to Equation 46,

$$m_v = \frac{K}{c_v r_f} \tag{43}$$

Therefore complete consolidation S under loading of 20 kPa is estimated to be

$$S = m_v \Delta\sigma' H_0 = 0.32 H_0 \tag{44}$$

where H_0 is the initial sample height. In other word, the final sample height of *0.6 m* equals to $0.68\mathrm{H}_0$, and the initial sample height is calculated $H_0 = 0.89\ m$ and initial slurry volume $V_0 = 1.57\ m^3$. Apart from that, to avoid air entrainment to the clay sample during the consolidation, a water layer of 11mm is kept above the sample surface from the beginning of consolidation.

Knowing the initial and final sample height as well as initial sample water content, the final water content is expected to be 69%, based on the weight balance of solids in the tank at the initial and final stage of consolidation, as shown in Equation 48. As documented by Martin (1994), low undrained shear strength normally corresponds to high water content in clay, and from the $w - Su$ trend line plotted by Martin (1994) based on experimental data from Gue (1984) and Martin (1994), it is reasonable to expect a water content of 69% at low strength level of 4 kPa, though a bit higher than the liquid limit 65%.

$$H_0 = \frac{H_1}{1 + G_s w_{,0}}(1 + G_s w_{,0}) \tag{45}$$

Where H_0=initial height of slurry in tank, m;

H_1= final height of clay sample in tank, m;

w_0= initial water content of clay in tank;

w_1= final water content of clay in tank.

5.3.4 Consolidation

The consolidation and unloading are performed under a sequence of loading stages: the initial loading is 20 kPa and then after 15 days it is reduced to 0 and remains at that level for 36 hours. The complete consolidation takes an expected time period computed from one dimensional consolidation theory (drainage path length $H_0/2$ due to top and bottom drainage):

$$T_v = \frac{C_v t}{(H_0/2)^2} \tag{46}$$

where dimensionless time factor T_v is expressed by Equation 50 (Knappett & Craig, 2012)

$$T_v = -0.933 log(1 - U_v) - 0.085 \tag{47}$$

Take $H_0 = 0.89$ m, $C_v = 4\ m^2/year$, $U_v = 0.90$ (very close to complete consolidation), the consolidation duration reaches t =15 days therefore it is taken as the loading period under 20 kPa. Dissipation of pore suction pressure takes 36 hours under 0 kPa as indicated by Gue (1988) and Martin (1994). However, these two suggested loading periods may not fit the real case in lab, therefore they are adjustable based on the criteria that, the loading stage of 20 kPa should last a long period enough to reach the end of primary consolidation with final sample depth being 0.6 m, and the unloading at 0 kPa should also maintain long to allow for the dissipation of suction pressure of the specimen. A real-time figure showing the sample height over time should be drawn to help identify the criteria.

Keep drainage valve always open during the whole consolidation period so that rapid consolidation occurs. With the loading-unloading process, the clay sample becomes overconsolidated clay and its undrained shear strength follows a distribution over depth depending on OCR and depth, see Equation 51. As predicted in Appendix E, the sample clay 0.42 m below soil surface (pile length) can be regarded as uniform clay with average undrained shear strength of 4 kPa.

On the other hand, the main task in sample preparation is to create clay with uniform undrained shear strength of 4 kPa, therefore the value of γ' is relatively less focused. But for completely consolidated clay, the value of γ'will not fluctuate much from a typical value, therefore γ' is considered to be the expected value of 15 kN/m^3.

$$S_u = 0.23\sigma_v' OCR^{0.8} \quad (48)$$

where

0.23, 0.8= typical coefficients, close to those proposed by Houlsby (1993);

σ_v'=effective vertical stress, $\sigma_v' = \gamma' H$

OCR=overconsolidated ratio, $OCR = \frac{20\ kPa + \gamma' H}{\gamma' H}$ in this case

γ'=effective unit weight after consolidation

5.4 Suction pile instillation

After the consolidation-swelling process, three suction piles are installed into the three clay tanks, though the installation is not via suction but by pushing instead. The expected vertical penetration of caissons can be achieved by applying hanger of 10 kg on the loading platen. Though it is generally believed that the installation method, suction versus pushing, determines resistance distribution along pile length, it imposes minor effect on the behaviour of the suction caissons (Zhu, Byrne, & Houlsby, 2012). The caissons are made of steel with dimension of $0.3\ m \times 0.42\ m$ (internal diameter × height) and thickness of 6 mm.

Since the lateral loading on caisson in lab is achieved via a horizontally laid steel cable attached to the caisson with loading point at 70% of the caisson height (see Figure 34), the installation of the cable should be considered at the time of pile installation. An innovative design of cable installation along with pile installation is attached in Figure 33, and concise description of the different installation stages is shown below.

During the stage in Figure 33-a, the slurry has not yet been pumped into the soil tank, and the cable is kept in position through several fixed pulleys with one cable end attached to the loading beam and another to the inner wall of the tank. The cable at this stage is in tension ensuring that pulleys hold it tightly. Connections between cable end and beam or tank wall is accomplished through hooks and eyes.

Figure 33-b indicates that, when the slurry has been transported into the container and the consolidation-swelling has taken place, the steel cable still remains tight.

At the beginning of pile installation as displayed in Figure 33-c, the hooks at the two cable ends are released from the loading beam and tank wall, and one end is manually attached to the padeye on the caisson. In this stage, the buried cable away from the caisson still keeps close connection with the buried pulley, thanks to the positioning of the overconsolidated clay.

Figure 33-d shows that the caisson drags down part of the attached cable during caisson installation process.

Eventually in Figure 33-e when the caisson penetrates to the expected depth, the cable is again hold tightly with one end fixed to loading beam while another one to suction caisson.

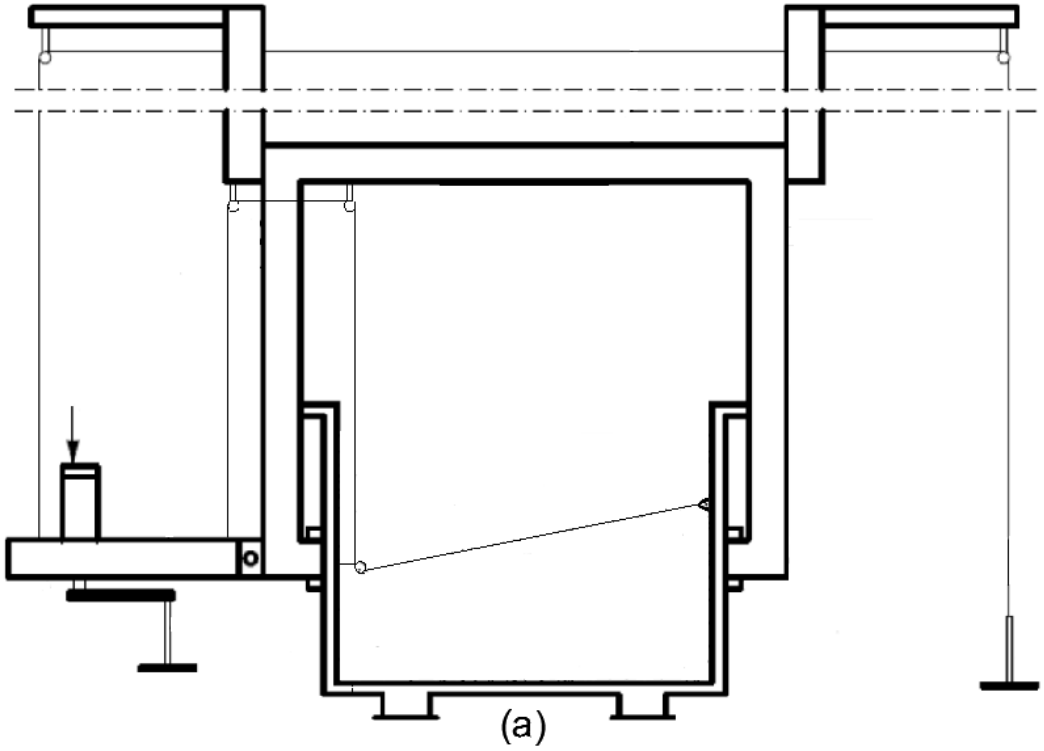
(a)

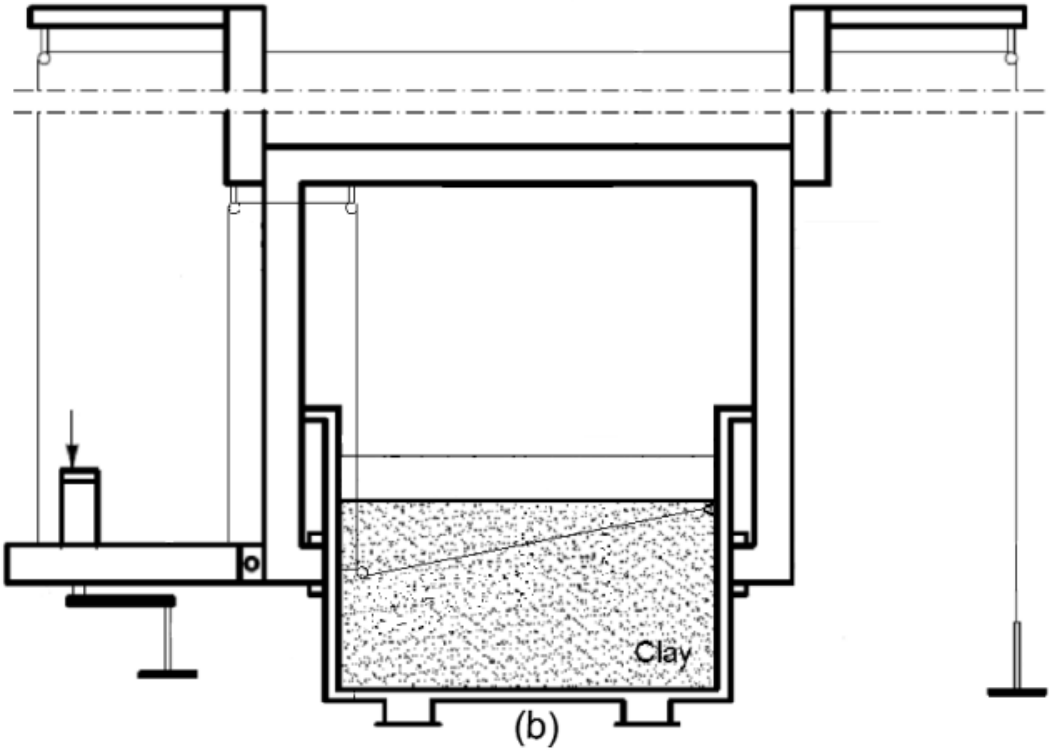
Clay
(b)

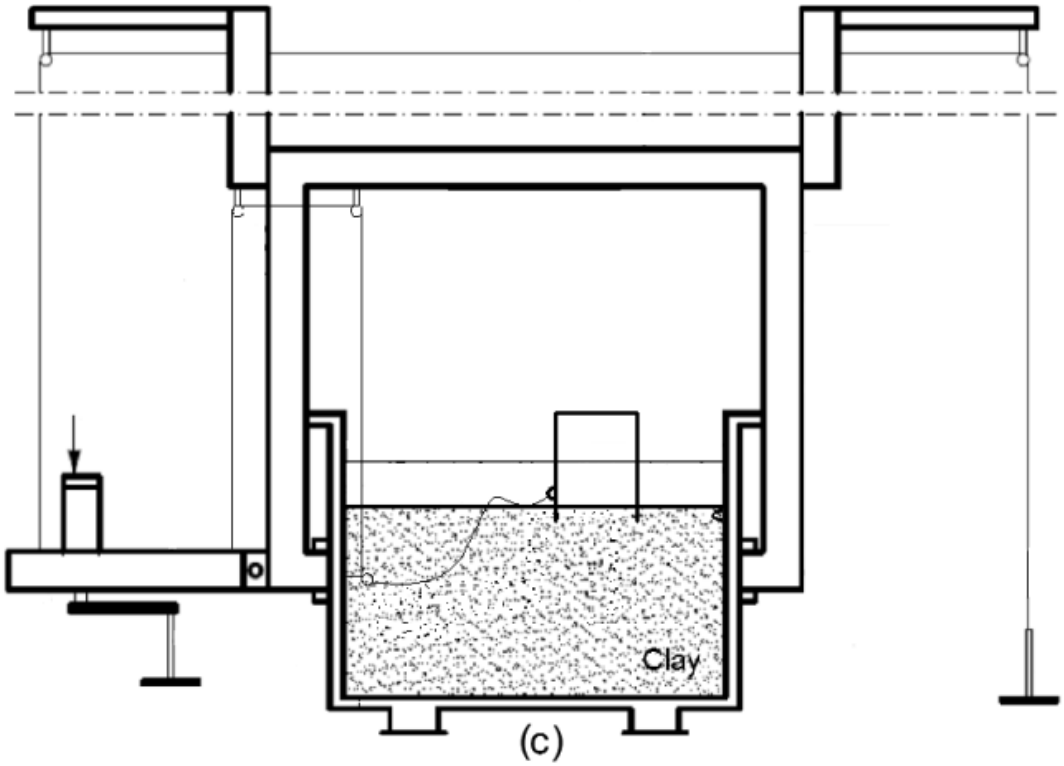

(c)

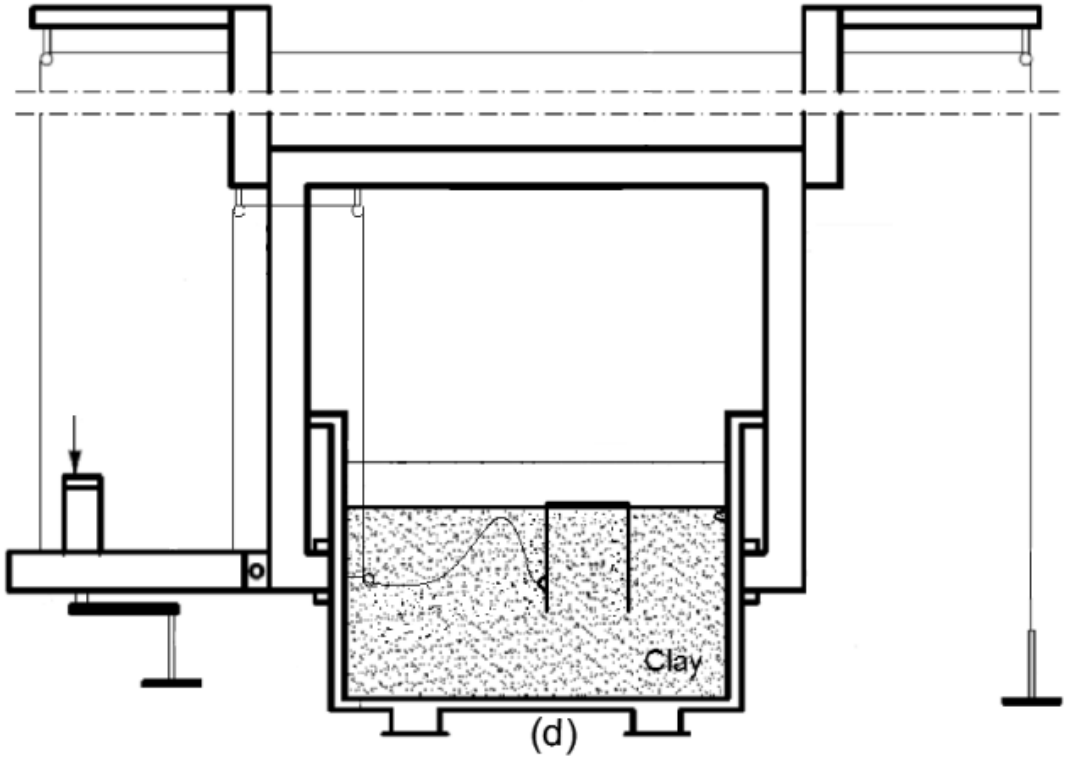

(d)

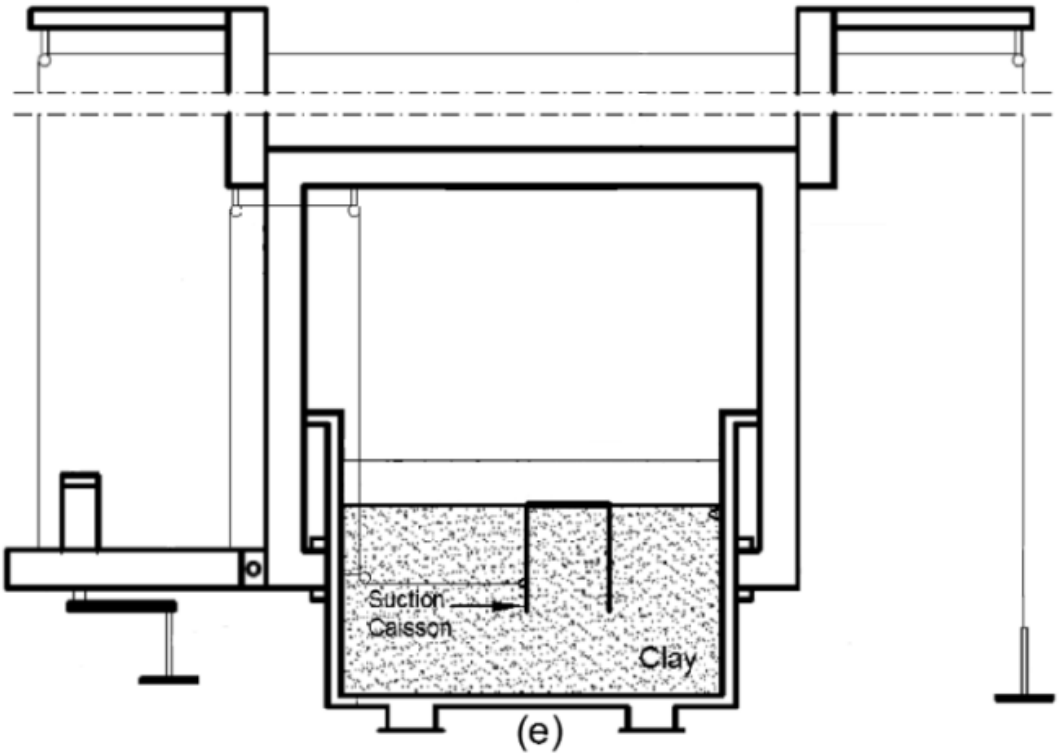

Figure 33 - Steps of loading cable installation along with caisson installation

5.5 Sample properties tests

Through careful calculation based on theoretical equations as well as empirical data, the exact undrained shear strength of the sample clay may, however, vary from the expected value, therefore sample properties tests are recommended to verify the expected strength after consolidation-unloading and after the pile driving. Proposed tests can be separated into two categories: In-situ tests and laboratory tests. Among In-situ tests, shear vane test is applied by researchers from Oxford, e.g., Gue (1984), Santa Maria (1988) and Martin (1994), to determine undrained shear strength profile. Mini CPT tests in the same samples can also be performed. Laboratory sample tests determining soil strength include triaxial test and direct shear test.

Besides, as indicated previously, laboratory odometer tests are strongly suggested to determine initial slurry height before consolidation. Also soil height test regarding the consolidation-swelling behaviour of the soil is also proposed to be recorded on site.

If the obtained properties in tests differ quite much from those expected, it is suggested to adjust samples preparation and consolidation until the expected properties are reached before performing loading tests on suction piles.

When operating sample properties tests, one should carefully consider issues such as applying site investigation or sampling test, sampling strategy, how to obtain undisturbed sample, how to introduce less impact on parent sample due to sampling or site test, how to create in-situ stress level, the time and cost etc.

5.6 Loading test

After pile installation, one can use the loading rig shown in Figure 33 to apply lateral loading to the caisson, no matter static or cyclic. Three loading patterns are separately applied to the three caissons in the soil tanks to investigate the cyclic loading effect on soil stiffness.

5.6.1 Loading apparatus

On the basis of the apparatus developed by Aalborg university (Foglia, Ibsen, Andersen, & Roesen, 2012), this test program will apply an experiment rig capable of imposing cyclic lateral loading on suction caisson with loading position completely controllable, see Figure 34.

An electric motor, mounted on the loading beam, generates power to rotate weight hanger 1 in a horizontal plane, thus creating cyclic loading on suction caisson through the cable line, according to the moment equilibrium of the loading beam. The weight hanger 2 is used to balance the self-weight of the motor and the loading beam.

If the distance between the rotating weight hanger 1 and the rotation axis of beam follows

$$L_0 = L_2 + L_3\, sin(wt) \tag{49}$$

The lateral loading on pile can be calculated to be

$$F = mg(L_2 + L_3\, sin(wt))/L_1 \tag{50}$$

Where m = weight of weight hanger 1;

L_1, L_2, L_3 = position parameters, see Figure 35. In particular, L_2, L_3 is adjustable while L_1 is completely fixed;

w = angular speed, expressed by $w = 2\pi/T$ where T_p is rotation period controlled by the electric motor.

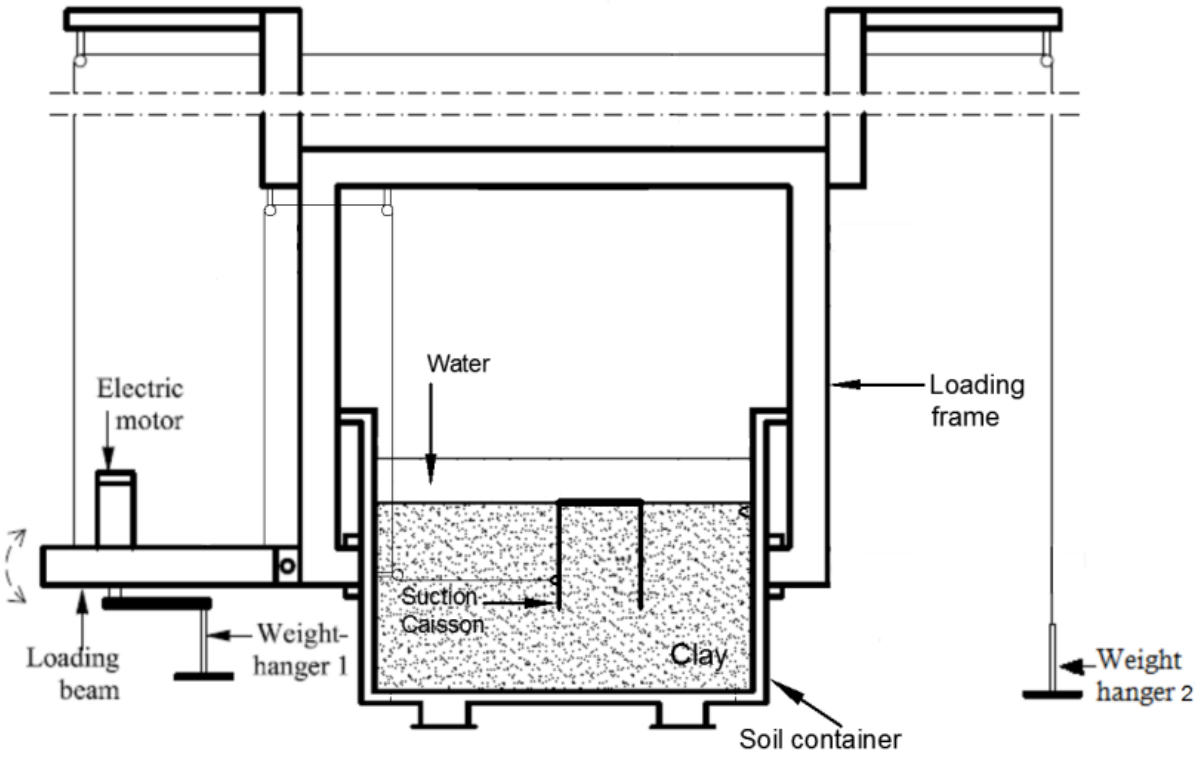

Figure 34 - Loading apparatus

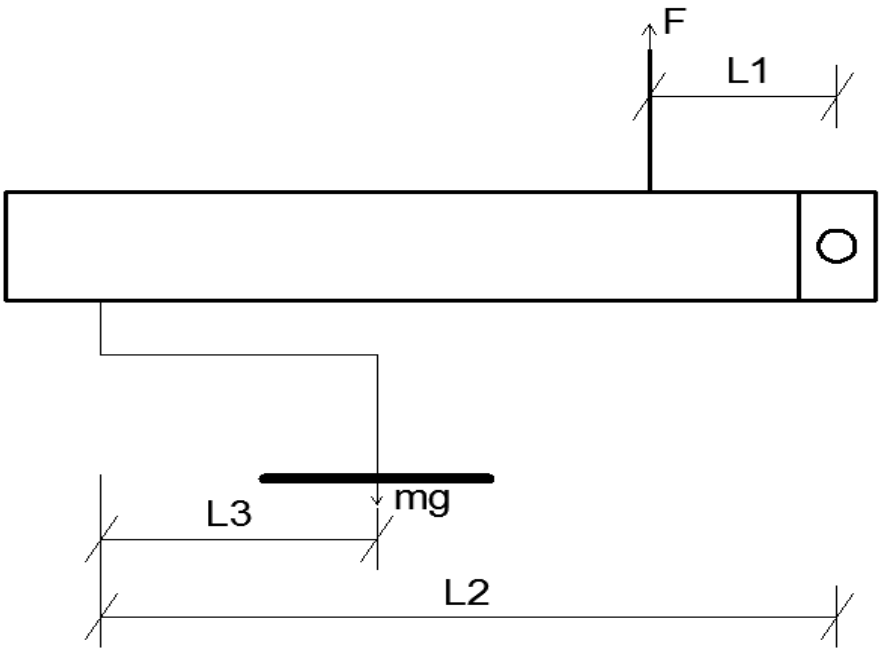

Figure 35 – Sketch of the loading beam

5.6.2 Loading procedures

Three loading scenarios respectively applied to the three suction caissons are under consideration. These tests aim to investigating the soil behaviour of horizontally loaded piles under cyclic loadings, and to verifying the *p-y* method used in Chapter 4.

5.6.2.1 Static test

This loading regime models static loading on caisson and is achieved at the existence of a weight hanger 1 fixed at the position (no motor in this case) where the distance between the hanger and rotation axial of beam remains L_2. Constant parameters include $m = 20.4\ kg, L_1 = 0.1\ m$. Adjust length L_2 to 0 m,0.25 m,0.5 m,0.75 m,1.0 m sequentially with a time interval of 1 day, thus creating lateral loading of 0 N,500 N,1000 N,1500 N,2000 N in laboratory which models a static load sequence of 0 kN,500 kN,1000 kN,1500 kN,2000 kN in prototype, if set the load scale $u_F = 1/1000$.

Record the displacement data after each one day, which corresponds to a prototype loading period of 33 days representing consolidation under short-term static loading condition. The measured displacement is scaled 10 times larger to predict the value in prototype according to dimensionless Equation 40. During the whole test the drainage outlet is always kept open, which simulates the likely drainage condition in field. In this way, the drainage is partially allowed but on the other hand, the drainage time is very much likely shorter than the consolidation time according to equation 46 and 47.

5.6.2.2 Cyclic test 1

The first cyclic test models a combination of prototypic mean load of 1540 kN and dynamic load of 227 kN, upon which the suction caisson with 4.2 meters length and 3 meters diameter is designed. To simulate this load pattern in laboratory, a load scale of $u_F = 1/1000$ is applied which refers to a mean load of 1540 N together with a dynamic load of 227 N in laboratory.

To obtain this load pattern, $m = 20.4\ kg, L_1 = 0.1\ m, L_2 = 0.77\ m, L_3 = 0.11\ m$. Besides, the electric motor should strictly control the rotation period $T = 22.6\ \text{minutes}$ corresponding to current period of 12 hours and 25 minutes in prototype. During the whole test the drainage outlet is always kept open.

Displacement data is recorded 20 days after the loading application so that 1270 loading cycles have been applied. In order to have a better view of the long term response, an experimental period of 6 months can be chosen, if possible, to apply over 10000 load cycles. To predict the displacement of prototype the recorded data should be scaled 10 times larger.

5.6.2.3 Cyclic test 2

The second cyclic test models a combination of prototype mean load of 1540 kN and dynamic load of 1540 kN, which represents the extreme case where the loading, although cyclic, is perfectly applied just in one direction. To simulate this load pattern in laboratory, a load scale of $u_F = 1/1000$ is applied which refers to a mean load of 1540 N in combination of a dynamic load of 1540 N.

To obtain this load pattern, $m = 20.4\,kg, L_1 = 0.1\,m, L_2 = 0.77\,m, L_3 = 0.77\,m$. Besides, the electric motor should well control the rotation period $T = 22.6\,minutes$ corresponding to current period of 12 hours and 25 minutes in prototype. During the whole test the drainage outlet is always kept open.

Displacement data is recorded 20 days after the loading application so that 1270 loading cycles have been applied. In order to have a better view of the long term response, an experimental period of 6 months can be chosen, if possible, to apply over 10000 load cycles. To predict the displacement of prototype the recorded data should be scaled 10 times larger.

5.6.3 Data analysis

After data collection during loading tests, three sets of load-displacement curve under different loading schemes should be plotted and compared with each other.

For static loading tests, the displacement results are scaled to predict the prototype results, which can be compared with those predicted by theoretic Equation 33. Moreover, a parametric study should be conducted by plotting the laboratory parameter $F/S_u D^2$ against laboratory parameter $(y/D)^{1/3}$, to verify the fundamental p-y equation which supports both analytical deformation analysis and experimental deflection analysis.

Furthermore, cyclic loading plots are compared with static loading plot to investigate the difference of soil behaviour when subjected to static loading and cyclic loading. Since the inclination of the load-displacement curve represents soil stiffness, a cycle-by-cycle study can also be performed to obtain the development of lateral soil stiffness after each loading cycle. A plot showing the soil stiffness against number of loading cycles can also be graphed to directly show the trend of lateral soil stiffness development under cyclic loading.

6 Conclusion

The application of suction caissons as foundation solution of submerged floating tunnels in the Sognefjord, Norway is explored in this thesis project. Based on offshore engineering practice as well as site-specific conditions, laterally loaded suction caissons connected with cables are designed for various loading scenarios that incorporate elements such as current event, cable layout, soil type, and soil strength profile. The design gives an overview of the caisson dimension for the submerged floating tunnels corresponding to these scenarios. The results indicate that a mooring system consisting of suction caissons and mooring cables are capable of keeping the floating tunnel in position with a reasonable caisson diameter D and length L (D = 3 - 5 m, L/D < 6 in most cases). Additionally, a parametric study of the static pile-soil deformation has been performed, indicating that more refined design method is required to satisfy serviceability limit.

Although the design for static, primarily horizontally, load cases is well established and presented in this thesis, the application of cyclic loads and its effect on the serviceability limit state is less well developed.

Hence, this thesis presents a rigorously designed 1-g physical model setup to test the cyclic response of a model suction caisson in laboratory clay. The test setup still has a reasonably small footprint and the sample preparation is reasonably quick (17 days, including mixing, consolidation and swelling). The mechanical loading apparatus originally developed by Foglia et al. (2012) is modified to facilitate cyclic loading on the suction pile at 70 percent of the pile length with a large number of 10000 load cycles in about half a year of testing time.

7 Bibliography

Aas-Jakobsen, Johs Holt, NGI, & Skanska. (2013). *Sognefjorden Feasibility Study of Floating Bridge.* Statens Vegvesen.

Andersen, K. H. (2009). Bearing capacity under cyclic loading-offshore, along the coast, and on land. The 21st Bjerrum Lecture presented in Oslo, 23 November 2007. *Canadian Geotechnical Journal, 46*(5), 513-535.

Andersen, K. H., & Jostad, H. P. (1999). Foundation design of skirted foundations and anchors in clay. *Offshore Technology Conference.*

Andersen, K. H., Murff, J. D., Randolph, M. F., Clucky, E. C., Erbrich, C. T., Jostad, H. P., et al. (2005). Suction anchors for deepwater applications. *Proc. Int. Symp. on Frontiers in Offshore Geotechnics (ISFOG)* (pp. 3-30). London: Taylor & Francis Group.

API. (2005). *Recommended Practice for Planning, Designing and Constructing Fixed Offshore Platform-Working Stress Design, 21st Edition.* Washington, D.C.: American Petroleum Institute.

Aubeny, C. P., Han, S. W., & Murff, J. D. (2003). Inclined load capacity of suction caissons. *International Journal for Numerical and Analytical Methods in Geomechanics, 27*(14), 1235-1254.

Aubeny, C. P., Murf, J. D., & Moon, S. K. (2001). Lateral undrained resistance of suction caisson anchors. *International Journal of Offshore and Polar Engineering, 11*(3), 211-219.

Aubeny, C., & Murff, J. D. (2005). Simplified limit solutions for the capacity of suction anchors under undrained conditions. *Ocean Engineering, 32*(7), 864-877.

Broms, B. B. (1964). Lateral resistance of piles in cohesive soils. *JSMFD, 90*(2), 123-156.

Chakrabarti, S. (2005). *Handbook of Offshore Engineering.* Elsevier.

DDBST. (n.d.). *Liquid dynamic viscosity*. Retrieved 2014, from http://ddbonline.ddbst.de/VogelCalculation/VogelCalculationCGI.exe

Deng, W., Carter, J. P., & Taiebat, H. (2001). Prediction of the Lateral Capacity of Suction Caissons. *Computer Methods and Advances in Geomechanics: Proceedings of the 10th International Conference on Computer Methods and Advances in Geomechanics* (pp. 33-38). Tucson, Arizona, USA: CRC Press.

DNV. (2005). *Geotechnical design and installation of suction anchors in clay.* DNV Recommended Practice RP-E303, Høvik.

El-Sherbiny, R., Vanka, S., Olson, R., & Gilbert, R. (2005). Capacity of suction caissons under inclined loading in normally consolidated clay. *Proceedings of the International Symposium on Frontiers in Offshore Geotechnics,* (pp. 281-287).

Foglia, A., Ibsen, L. B., Andersen, L. V., & Roesen, H. R. (2012). Physical Modelling of Bucket Foundation under Long-Term Cyclic Lateral Loading. *Proceedings of the 22nd International Offshore and Polar Engineering Conference* (pp. 667-673). ISOPE.

Gue, S. S. (1984). *Ground heave around driven piles in clay.* Doctoral dissertation, University of Oxford.

Huang, J., Cao, J., & Audibert, J. (2003). Geotechnical Design of Suction Caisson in Clay. *In The Thirteenth International Offshore and Polar Engineering Conference*. Hawaii, USA: International Society of Offshore and Polar Engineers.

Kartverket. (2014a). *Currents*. Retrieved 2014, from Vannstand.no: http://vannstand.no/index.php/nb/english-articles/currents

Kartverket. (2014b). *Tide table*. Retrieved 2014, from http://vannstand.no/index.php/nb/english-section/tide-table

Kartverket. (2014c). *Tidal Level – Ålesund*. Retrieved 2014, from http://vannstand.no/index.php/english-section/index.php?option=com_content&view=article&Itemid=102&id=205%3Atidal-level-alesund

Kelly, R. B., Houlsby, G. T., & Byrne, B. W. (2006). A comparison of field and laboratory tests of caisson foundations in sand and clay. *Géotechnique, 56*(9), 617-626.

Knappett, J., & Craig, R. F. (2012). *Craig's Soil Mechanics* (8th ed.). Spon Press.

LeBlanc, C., Houlsby, G. T., & Byrne, B. W. (2009). Response of stiff piles in sand to long-term cyclic lateral loading. *Géotechnique, 60*(2), 79-90.

Martin, C. M. (1994). *Physical and numerical modelling of offshore foundations under combined loads.* Doctoral dissertation, University of Oxford.

Math24.Net. (2014). *Equation of Catenary*. Retrieved from http://www.math24.net/equation-of-catenary.html

Matlock, H. (1970). Correlations for design of laterally loaded piles in soft clay. *Offshore Technology in Civil Engineering's Hall of Fame Papers from the Early Years*, 77-94.

Muir Wood, D. (2004). *Geotechnical modelling* (1st ed.). London and New York: CRC Press.

Murff, J. D., & Hamilton, J. M. (1993). P-Ultimate for undrained analysis of laterally loaded piles. *Journal of Geotechnical Engineering, 119*(1), 91-107.

NGI. (2014). *Skirted Caisson Foundations for Offshore Structure*. Retrieved from NGI: http://www.ngi.no/no/Innholdsbokser/Referansjeprosjekter-LISTER-/Referanser/Skirted-Caisson-Foundations-for-Offshore-Structures/

Pradhan, D. L. (2012). *Master thesis project-Development of P-Y Curves for Monopiles in Clay using Finite Element Model Plaxis 3D Foundation.* Norwagian University of Science and Technology.

Randolph, M. F., & Houlsby, G. T. (1984). The limiting pressure on a circular pile loaded laterally in cohesive soil. *Geotechnique, 34*(4), 613-623.

Randolph, M. F., & House, A. R. (2002). Analysis of suction caisson capacity in clay. *Offshore Technology Conference.*

Randolph, M., & Gourvenec, S. (2011). *Offshore Geotechnical Engineering.* New York: Spon Press.

Randolph, M., Cassidy, M., Gourvenec, S., & Erbrich, C. (2005). Challenges of offshore geotechnical engineering. *Proceedings of the International Conference on Soil Mechanics and Geotechnical Engineering. 1*, pp. 123-176. Rotterdam, the Netherlands: Millpress Science Publishers.

Reese, L. C., Cox, W. R., & Koop, F. D. (1975). Field testing and analysis of laterally loaded piles on stiff clay. *Offshore Technology Conference.*

Reinertsen Olav Olsen Group. (2012, November 28). *Feasibility study for crossing the Sognefjord Submerged Floating Tunnel.* Statens Vegvesen.

Santa Maria, P. d. (1988). *Behaviour of footings for offshore structures under combined loads.* Doctoral thesis. University of Oxford.

Senders, M., & Kay, S. (2002). Geotechnical suction pile anchor design in deep water soft clays. *Conference Deepwater Risers, Moorings and Anchorings. 10*, pp. 2002-1. London: Fugro Engineers BV Veurse Achterweg.

Statens Vegvesen. (2013, August 21). *Fjord crossings*. Retrieved March 1, 2014, from http://www.vegvesen.no/Vegprosjekter/ferjefriE39/english/fjordcrossings

Supachawarote, C., Randolph, M., & Gourvenec, S. (2004). Inclined pull-out capacity of suction caissons. *The Fourteenth International Offshore and Polar Engineering Conference*. International Society of Offshore and Polar Engineers.

TUDelft. (2014). *Suction Anchors*. Retrieved 2014, from http://www.offshoremoorings.org/moorings/2006/Groep7/index_bestanden/Page498.htm

Zhu, B., Byrne, B. W., & Houlsby, G. T. (2012). Long-term lateral cyclic response of suction caisson foundations in sand. *Journal of Geotechnical and Geoenvironmental Engineering*, *139*(1), 73-83.

Appendix A Mooring cable pre-tension and dimension

The mooring cable in this project is taken as catenary line (see Figure 5) which is shaped by equation according to (Math24.Net, 2014):

$$Y = acosh(X/a) \tag{51}$$

Where Y, X – the y and x coordinates in a crossing coordinate system;

a – a parameter which satisfies $a = T_h/(\rho_{material} gA)$, where;

T_h – horizontal component of pre-tension in the cable line;

$\rho_{material}$ – cable material density;

A –area of cable line.

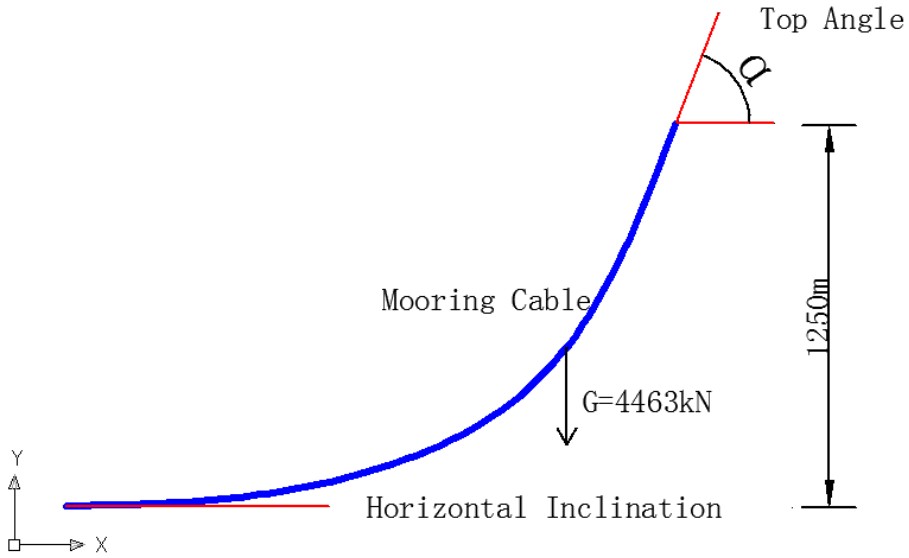

Figure 5 – Mooring cable layout

In this project three conditions are known or simplified:

1. Though the full picture of bottom topography is not available, we can still assume that for the interested tunnel section the mooring depth is 1250m.
2. The cable lies horizontally at the lower end.
3. The vertical tension component at the top end is $T_{v\_top} = G = 4463kN$.

The top angle α considered includes 71, 45 and 37 degree, and each angle value will result in one cable layout in terms of cable material, cable size and cable length.

Here a specific example for a 71 degree angle to horizontal at the cable top end is illustrated (without considering dynamic current loading effect). The analysis makes full use of algebra geometry provided by Math24.Net (2014).

$Tan(\alpha)$ refers to the derivative of line function $Y = acosh(X/a)$ at the top point, i.e.,

$$\left(\frac{dY}{dX}\right)_{top} = Tan(\alpha) = Tan(71^{\circ}) = 2.90 \quad (52)$$

Therefore

$$sinh\left(X_{top}/a\right) = 2.90 \quad (53)$$

Then it can be easily calculated that at the top end the *X* coordinate satisfies

$$X_{top}/a = 2.84 \quad (54)$$

If set the *X* coordinate of the lower end of cable line as *0*, it yields:

$$X_{low} = 0;\ Y_{low} = a \quad (55)$$

Since the water depth is assumed to be 1250m, it can be easily obtained that at the top end, the *Y* coordinate yields

$$Y_{top} = 1250 + a \quad (56)$$

Insert Equation 59 into shape function 54,

$$1250 + a = a \times cosh(2.84) \quad (57)$$

Solve Equation 60 iteratively (see Table 8) and the results show that

$$a \approx 605m$$

Table 8 - Iteration of cable layout parameter ***a*** for cable top angle of 71 degree

a (m)	***1250+a (m)***	$acosh(X_{top}/a)$
1	1251	3
2	1252	6
5	1255	15
10	1260	31
100	1350	306
605	1855	1853

Now choose the cable properties based on shape function.

At the top end $Tan(\alpha) = 2.90$, therefore

$$T_h = T_v/2.90 = 4463/2.90 = 1541kN$$

From $a = T_h/(\rho_{material} gA)$

$$\rho_{material} gA = T_h/a = 1541/605 = 2.55kN/m$$

$$\rho_{material} A = 2.55kN/10 = 255kg/m$$

Based on the value of $\rho_{material} A$, choose 3 sets of *Xtreme Spiral Strand* with the following properties:

Table 9 - Cable properties for top cable angle of 71 degree

Diameter 153 mm
Minimum Breaking Load 22070 kN
Submerged weight 95.5 kg/m
Axial stiffness 2110 MN
Cable horizontal length x=1.87*a=1080m
Total length s=1752m
Maximum cable force = equation=5424kN
Strength utilization=5424/(3*22070)=8%

The actual submerged weight of 3 spiral strands reaches 287 kg/m, a bit larger than the required 255kg/m, but the vertical balance of tunnel can still be kept by appropriately adjusting the amount of water or solid ballast in the tunnel tube. The results of the cable properties are summarized in Table 5 in Chapter 3.1.

For other angles at top end, the calculation process remains the same and the results are shown in Table 5 in Chapter 3.1. Below Table 10 and Table 11 show the iteration process determining parameter a in the Excel sheet.

Table 10 - Iteration of cable layout parameter ***a*** for cable top angle of 45 degree

a (m)	***1250+a (m)***	$acosh(X_{top}/a)$
1	1251	1
2	1252	3
5	1255	7
10	1260	14

100	1350	141
605	1855	856
800	2050	1131
3020	4270	4271

Table 11 - Iteration of cable layout parameter ***a*** for cable top angle of 37 degree

a (m)	***1250+a (m)***	$acosh(X_{top}/a)$
1	1251	1
2	1252	2
5	1255	6
10	1260	12
100	1350	125
605	1855	754
800	2050	997
5100	6350	6356

Appendix B Pile dimension for uniform clay under various combinations of current event and top cable angle

The lateral loaded pile design is based on the coupling between pile dimension and soil strength as demonstrated in Chapter 3.3.3, from Equation 21, 22 and 23.

$$R_{shallow} = \int_0^{Z_R} N_p S_u D dZ = 6 S_u D Z_R \tag{21}$$

$$\mathrm{R_{deep}} = 9\mathrm{S_u D(L - Z_R)} \tag{22}$$

$$R_u = R_{shallow} + R_{deep} \tag{23}$$

Firstly an example design is illustrated when the soil specific weight is 20 kN/m^2. Prescribe the uniform soil strength Su and pile diameter D, and calculate the critical depth ZR through Equation 18, and obtain length L by solving Equation 23 iteratively.

Note that when $L < Z_R$, the resistance is only provided by the soil above the critical depth and *Pu* will never reach 9*SuD*, therefore the total resistance should be adjusted by

$$R_u = \int_0^{L} N_p S_u D dZ = (3 + 3\,L/Z_R) S_u D, \qquad L < Z_R \tag{58}$$

The calculation results for various combinations of tide event, current event, top cable angle, soil strength and diameter are displayed in the following Table 12.

Table 12 - Pile dimension for uniform clay under 100 year tide and 50 year current and 71 degree top cable angle

Su(kpa)	D (m)	L (m)	L/D	cable load(KN)	Z_R (m)
15	3	13.2	4.4	4008	4.1
20	3	10.7	3.6	4008	5.3
25	3	9.3	3.1	4008	6.4
30	3	8.4	2.8	4008	7.5
35	3	7.0	2.3	4008	8.5
40	3	6.6	2.2	4008	9.5
15	4	10.3	2.6	4008	4.2

20	4	8.5	2.1	4008	5.5
25	4	7.6	1.9	4008	6.7
30	4	6.2	1.6	4008	7.8
35	4	5.8	1.4	4008	8.9
40	4	5.4	1.4	4008	10.0
15	5	8.5	1.7	4008	4.2
20	5	7.2	1.4	4008	5.6
25	5	5.8	1.2	4008	6.8
30	5	5.4	1.1	4008	8.0
35	5	5.0	1.0	4008	9.2
40	5	4.6	0.9	4008	10.3

Table 13 - Pile dimension for uniform clay under 100 year tide and 1 year current and 71 degree top cable angle

Su(kpa)	D	L	L/D	cable load(KN)	ZR (m)
15	3	7.7	2.6	2152	4.1
20	3	6.5	2.2	2152	5.3
25	3	5.3	1.8	2152	6.4
30	3	4.9	1.6	2152	7.5
35	3	4.0	1.3	2152	8.5
40	3	4.2	1.4	2152	9.5
15	4	6.2	1.5	2152	4.2
20	4	4.8	1.2	2152	5.5
25	4	4.3	1.1	2152	6.7
30	4	4.0	1.0	2152	7.8
35	4	3.7	0.9	2152	8.9
40	4	3.4	0.8	2152	10.0
15	5	5.2	1.0	2152	4.2
20	5	4.1	0.8	2152	5.6
25	5	3.7	0.7	2152	6.8

30	5	3.4	0.7	2152	8.0
35	5	3.1	0.6	2152	9.2
40	5	2.8	0.6	2152	10.3

Table 14 - Pile dimension for uniform clay under 100 year tide and 50 year current and 45 degree top cable angle

Su(kpa)	D (m)	L (m)	L/D	cable load(KN)	ZR (m)
15	3	24.5	8.2	7806	4.1
20	3	19.1	6.4	7806	5.3
25	3	16.0	5.3	7806	6.4
30	3	14.1	4.7	7806	7.5
35	3	12.7	4.2	7806	8.5
40	3	11.8	3.9	7806	9.5
15	4	18.7	4.7	7806	4.2
20	4	14.8	3.7	7806	5.5
25	4	12.6	3.2	7806	6.7
30	4	11.3	2.8	7806	7.8
35	4	10.4	2.6	7806	8.9
40	4	8.7	2.2	7806	10.0
15	5	15.3	3.1	7806	4.2
20	5	12.3	2.5	7806	5.6
25	5	10.6	2.1	7806	6.8
30	5	9.6	1.9	7806	8.0
35	5	8.0	1.6	7806	9.2
40	5	7.5	1.5	7806	10.3

Table 15 - Pile dimension for uniform clay under 100 year tide and 1 year current and 45 degree top cable angle

Su(kpa)	D	L	L/D	cable load(KN)	ZR (m)

15	3	19.0	6.3	5949	4.1
20	3	15.0	5.0	5949	5.3
25	3	12.7	4.2	5949	6.4
30	3	11.3	3.8	5949	7.5
35	3	10.4	3.5	5949	8.5
40	3	9.8	3.3	5949	9.5
15	4	14.6	3.7	5949	4.2
20	4	11.7	2.9	5949	5.5
25	4	10.2	2.5	5949	6.7
30	4	9.2	2.3	5949	7.8
35	4	7.6	1.9	5949	8.9
40	4	7.2	1.8	5949	10.0
15	5	12.0	2.4	5949	4.2
20	5	9.8	2.0	5949	5.6
25	5	8.6	1.7	5949	6.8
30	5	8.0	1.6	5949	8.0
35	5	6.6	1.3	5949	9.2
40	5	6.2	1.2	5949	10.3

Table 16 - Pile dimension for uniform clay under 100 year tide and 50 year current and 37 degree top cable angle

Su(kpa)	D (m)	L (m)	L/D	cable load(KN)	ZR (m)
15	3	30.4	10.1	9804	4.1
20	3	23.6	7.9	9804	5.3
25	3	19.6	6.5	9804	6.4
30	3	17.0	5.7	9804	7.5
35	3	15.3	5.1	9804	8.5
40	3	14.1	4.7	9804	9.5
15	4	23.2	5.8	9804	4.2
20	4	18.2	4.5	9804	5.5

25	4	15.3	3.8	9804	6.7
30	4	13.5	3.4	9804	7.8
35	4	12.3	3.1	9804	8.9
40	4	11.5	2.9	9804	10.0
15	5	18.8	3.8	9804	4.2
20	5	14.9	3.0	9804	5.6
25	5	12.7	2.5	9804	6.8
30	5	11.4	2.3	9804	8.0
35	5	10.5	2.1	9804	9.2
40	5	8.6	1.7	9804	10.3

Table 17 - Pile dimension for uniform clay under 100 year tide and 1 year current and 37 degree top cable angle

Su(kpa)	D	L	L/D	cable load(KN)	ZR (m)
15	3	24.9	8.3	7948	4.1
20	3	19.4	6.5	7948	5.3
25	3	16.3	5.4	7948	6.4
30	3	14.3	4.8	7948	7.5
35	3	12.9	4.3	7948	8.5
40	3	12.0	4.0	7948	9.5
15	4	19.1	4.8	7948	4.2
20	4	15.1	3.8	7948	5.5
25	4	12.8	3.2	7948	6.7
30	4	11.4	2.9	7948	7.8
35	4	10.5	2.6	7948	8.9
40	4	10.0	2.5	7948	10.0
15	5	15.5	3.1	7948	4.2
20	5	12.4	2.5	7948	5.6
25	5	10.8	2.2	7948	6.8
30	5	9.7	1.9	7948	8.0

35	5	8.1	1.6	7948	9.2
40	5	7.6	1.5	7948	10.3

Appendix C Pile dimension for normally consolidated clay under various combinations of current event and top cable angle

The lateral loaded pile design is based on the coupling between pile dimension and soil strength as demonstrated in Chapter 3.3.3, from Equation 23, 28 and 29:

$$R_{shallow} = \frac{1}{3}JkZ_R{}^3 + \left(\frac{3}{2}Dk + \frac{1}{2}\gamma D + \frac{1}{2}JS_{u0}\right)Z_R{}^2 + 3DS_{u0}Z_R \qquad (28)$$

$$\mathrm{R_{deep}} = \frac{9}{2}\mathrm{D}(2S_{\mathrm{u0}} + \mathrm{k}Z_R + \mathrm{kL}) \qquad (29)$$

Assume that the soil specific weight is always 20 kN/m^2. Prescribe the initial soil strength S_{u0} and gradient k and pile diameter D, and calculate iteratively the critical depth Z_R through Equation 25 and obtain length L by solving equation 23 iteratively.

Note that when $L < Z_R$, the resistance is only provided by the soil above the critical depth and *Pu* will never reach 9*SuD*, therefore the resistance should be adjusted by

$$R_u = \frac{1}{3}JkL^3 + \left(\frac{3}{2}Dk + \frac{1}{2}\gamma D + \frac{1}{2}JS_{u0}\right)L^2 + 3DS_{u0}L \qquad (59)$$

The calculation results for various combinations of tide event, current event, top cable angle, soil strength and pile diameter are displayed in the following Table 18.

Table 18 - Pile dimension for normally consolidated clay under 100 year tide and 50 year current and 71 degree top cable angle

k (kN/m^3)	Su0	D (m)	L (m)	L/D	cable load(kN)	ZR (m)
1	5	4	11.0	2.7	4008	2.0
1.5	5	4	9.5	2.4	4008	2.5
2	5	4	8.6	2.1	4008	3.3
2.5	5	4	8.0	2.0	4008	4.5
3	5	4	7.6	1.9	4008	6.6
3.5	5	4	7.4	1.9	4008	10
1	5	5	9.5	1.9	4008	2.1
1.5	5	5	8.3	1.7	4008	2.6
2	5	5	7.6	1.5	4008	3.4
2.5	5	5	7.0	1.4	4008	4.7

3	5	5	6.8	1.4	4008	7.3
3.5	5	5	6.6	1.3	4008	11.5
1	5	6	8.4	1.4	4008	2.1
1.5	5	6	7.4	1.2	4008	2.6
2	5	6	6.8	1.1	4008	3.4
2.5	5	6	6.4	1.1	4008	4.9
3	5	6	6.2	1.0	4008	7.8
3.5	5	6	6.0	1.0	4008	12.9

Table 19 - Pile dimension for normally consolidated clay under 100 year tide and 50 year current and 71 degree top cable angle

k (kN/m^3)	Su0	D (m)	L (m)	L/D	cable load(kN)	ZR (m)
1	5	4	7.3	1.8	2152	2.0
1.5	5	4	6.5	1.6	2152	2.5
2	5	4	6.0	1.5	2152	3.3
2.5	5	4	5.6	1.4	2152	4.5
3	5	4	5.5	1.4	2152	6.6
3.5	5	4	5.3	1.3	2152	10
1	5	5	6.3	1.3	2152	2.1
1.5	5	5	5.6	1.1	2152	2.6
2	5	5	5.2	1.0	2152	3.4
2.5	5	5	5.0	1.0	2152	4.7
3	5	5	4.9	1.0	2152	7.3
3.5	5	5	4.8	1.0	2152	11.5
1	5	6	5.6	0.9	2152	2.1
1.5	5	6	5.0	0.8	2152	2.6
2	5	6	4.7	0.8	2152	3.4
2.5	5	6	4.5	0.8	2152	4.9
3	5	6	4.4	0.7	2152	7.8

3.5	5	6	4.3	0.7	2152	12.9

Table 20 - Pile dimension for normally consolidated clay under 100 year tide and 50 year current and 45 degree top cable angle

k (kN/m^3)	Su0	D (m)	L (m)	L/D	cable load(kN)	ZR (m)
1	5	4	16.6	4.1	7806	2.0
1.5	5	4	14.2	3.5	7806	2.5
2	5	4	12.6	3.2	7806	3.3
2.5	5	4	11.6	2.9	7806	4.5
3	5	4	10.8	2.7	7806	6.6
3.5	5	4	10.4	2.6	7806	10
1	5	5	14.5	2.9	7806	2.1
1.5	5	5	12.4	2.5	7806	2.6
2	5	5	11.1	2.2	7806	3.4
2.5	5	5	10.2	2.0	7806	4.7
3	5	5	9.6	1.9	7806	7.3
3.5	5	5	9.3	1.9	7806	11.5
1	5	6	12.9	2.2	7806	2.1
1.5	5	6	11.1	1.9	7806	2.6
2	5	6	10.0	1.7	7806	3.4
2.5	5	6	9.2	1.5	7806	4.9
3	5	6	8.8	1.5	7806	7.8
3.5	5	6	8.5	1.4	7806	12.9

Table 21 - Pile dimension for normally consolidated clay under 100 year tide and 1 year current and 45 degree top cable angle

k (kN/m^3)	Su0	D (m)	L (m)	L/D	cable load(kN)	ZR (m)
1	5	4	14.0	3.5	5949	2.0

1.5	5	4	12.1	3.0	5949	2.5
2	5	4	10.8	2.7	5949	3.3
2.5	5	4	9.9	2.5	5949	4.5
3	5	4	9.4	2.3	5949	6.6
3.5	5	4	9.0	2.3	5949	10
1	5	5	12.2	2.4	5949	2.1
1.5	5	5	10.6	2.1	5949	2.6
2	5	5	9.5	1.9	5949	3.4
2.5	5	5	8.8	1.8	5949	4.7
3	5	5	8.3	1.7	5949	7.3
3.5	5	5	8.1	1.6	5949	11.5
1	5	6	10.9	1.8	5949	2.1
1.5	5	6	9.5	1.6	5949	2.6
2	5	6	8.6	1.4	5949	3.4
2.5	5	6	7.9	1.3	5949	4.9
3	5	6	7.6	1.3	5949	7.8
3.5	5	6	7.4	1.2	5949	12.9

Table 22 - Pile dimension for normally consolidated clay under 100 year tide and 50 year current and 37 degree of top cable angle

k (kN/m^3)	Su0	D (m)	L (m)	L/D	cable load(kN)	ZR (m)
1	5	4	19.0	4.8	9804	2.0
1.5	5	4	16.2	4.0	9804	2.5
2	5	4	14.4	3.6	9804	3.3
2.5	5	4	13.1	3.3	9804	4.5
3	5	4	12.2	3.1	9804	6.6
3.5	5	4	11.6	2.9	9804	10
1	5	5	16.6	3.3	9804	2.1
1.5	5	5	14.2	2.8	9804	2.6

2	5	5	12.7	2.5	9804	3.4
2.5	5	5	11.6	2.3	9804	4.7
3	5	5	10.9	2.2	9804	7.3
3.5	5	5	10.5	2.1	9804	11.5
1	5	6	14.9	2.5	9804	2.1
1.5	5	6	12.8	2.1	9804	2.6
2	5	6	11.4	1.9	9804	3.4
2.5	5	6	10.5	1.7	9804	4.9
3	5	6	9.9	1.6	9804	7.8
3.5	5	6	9.6	1.6	9804	12.9

Table 23 - Pile dimension for normally consolidated clay under 100 year tide and 1 year current and 37 degree top cable angle

k (kN/m^3)	Su0	D (m)	L (m)	L/D	cable load(kN)	ZR (m)
1	5	4	16.8	4.2	7948	2.0
1.5	5	4	14.3	3.6	7948	2.5
2	5	4	12.8	3.2	7948	3.3
2.5	5	4	11.7	2.9	7948	4.5
3	5	4	10.9	2.7	7948	6.6
3.5	5	4	10.5	2.6	7948	10
1	5	5	14.6	2.9	7948	2.1
1.5	5	5	12.6	2.5	7948	2.6
2	5	5	11.2	2.2	7948	3.4
2.5	5	5	10.3	2.1	7948	4.7
3	5	5	9.7	1.9	7948	7.3
3.5	5	5	9.4	1.9	7948	11.5
1	5	6	13.1	2.2	7948	2.1
1.5	5	6	11.3	1.9	7948	2.6
2	5	6	10.1	1.7	7948	3.4

2.5	5	6	9.3	1.6	7948	4.9
3	5	6	8.8	1.5	7948	7.8
3.5	5	6	8.6	1.4	7948	12.9

Appendix D Sample construction of the F-y curve

The pile-soil interaction can be modeled with Equation 33 in Chapter 4.2 as

$$\frac{F}{R_u} = 0.5\left(\frac{y}{y_c}\right)^{1/3} \quad (33)$$

R_u has been calculated as design line tension in Chapter 3.2, and y_c can be calculated as 0.2D as demonstrated in Chapter 4.2, Given a value F, a corresponding value of y can be easily obtained with Equation 33. Some pile dimensions are chosen to analyze the pile-soil interaction, and the effects of pile length, soil undrained shear strength are individually studied, see Figure 24-29. Here only part of the results for pile installed in uniform clay is shown.

Table 24 - Predicted load-deflection curve for various loading capacity (uniform clay)

Su (kpa)	D (m)	L (m)	L/D	cable load (KN)	yc (m)	F	F/Fu	P/Pu	y/yc	y (m)
20	3	10.7	3.6	4008	0.06	0	0.000	0.000	0.000	0.000
						500	0.125	0.125	0.016	0.001
						1000	0.250	0.250	0.124	0.007
						1500	0.374	0.374	0.419	0.025
						2000	0.499	0.499	0.994	0.060
						2500	0.624	0.624	1.942	0.117
						3000	0.749	0.749	3.356	0.201
						3500	0.873	0.873	5.329	0.320
						4000	0.998	0.998	7.954	0.477
						4008	1.000	1.000	8.000	0.480
						4008				1.000
20	5	7.2	1.4	4008	0.1	0	0.000	0.000	0.000	0.000
						500	0.125	0.125	0.016	0.002
						1000	0.250	0.250	0.124	0.012
						1500	0.374	0.374	0.419	0.042

						2000	0.499	0.499	0.994	0.099
						2500	0.624	0.624	1.942	0.194
						3000	0.749	0.749	3.356	0.336
						3500	0.873	0.873	5.329	0.533
						4000	0.998	0.998	7.954	0.795
						4008	1.000	1.000	8.000	0.800
						4008				1.000
30	3	14.1	4.7	7806	0.06	0	0.000	0.000	0.000	0.000
						1000	0.128	0.128	0.017	0.001
						2000	0.256	0.256	0.135	0.008
						3000	0.384	0.384	0.454	0.027
						4000	0.512	0.512	1.077	0.065
						5000	0.641	0.641	2.103	0.126
						6000	0.769	0.769	3.634	0.218
						7000	0.897	0.897	5.770	0.346
						7806	1.000	1.000	8.000	0.480
						7806				1.000
20	3	23.6	7.9	9804	0.06	0	0.000	0.000	0.000	0.000
						1000	0.102	0.102	0.008	0.001
						2000	0.204	0.204	0.068	0.004
						3000	0.306	0.306	0.229	0.014
						4000	0.408	0.408	0.543	0.033
						5000	0.510	0.510	1.061	0.064
						6000	0.612	0.612	1.834	0.110
						7000	0.714	0.714	2.912	0.175
						8000	0.816	0.816	4.347	0.261
						9000	0.918	0.918	6.189	0.371
						9804	1.000	1.000	8.000	0.480
						9804				1.000

Appendix E Predicted undrained shear strength of overconsolidated clay in laboratory

Table 25 - Predicted undrained shear strength profile of overconsolidated clay created in laboratory

Effective unit weight γ' ***(kN/m3)***	**Depth** *Z* ***(m)***	**Undrained shear strength** *Su* ***(kPa)***
15	0.1	3.0
15	0.2	3.5
15	0.3	4.0
15	0.4	4.5
15	0.5	4.8
Averagely uniform strength		4.0